



Optimal design and performance analysis of coastal microgrid using different optimization algorithms

Abualkasim Bakeer¹ · Mahmoud F. Elmorshedy^{2,3} · Hossam S. Salama¹ · Mohamed R. Elkadeem⁴ · Dhafer J. Almakhlis³ · Kotb M. Kotb²

Received: 17 November 2022 / Accepted: 17 July 2023 / Published online: 28 August 2023
© The Author(s) 2023

Abstract

Owing to the stochastic behavior of renewable energy activity and the multiple design considerations, the advancement of hybrid renewable energy-based microgrid (HREMG) systems has become a complex task. This study proposes a design optimization algorithm for the long-term operation of an autonomous HREMG along with the optimal system capacities. The investigated energy system comprises photovoltaic panels, wind turbines, diesel generators, and batteries. It aims to energize a remote coastal community with a daily load demand of 400 kWh in Marsa Matruh, Egypt. Since most studies utilize commercial tools in the design optimization procedure, the African vultures optimization approach (AVOA) is developed to find the optimal energy alternative and determine the optimal component's capacity considering achieving the minimum energy cost and loss of power supply probability. Moreover, an adequate energy management strategy is suggested to coordinate the power flow within the energy system in which renewable energy sources are fully penetrated. To check the AVOA robustness and efficacy, its performance is compared with the HOMER Pro most popular commercial tool as well as with new metaheuristic algorithms, namely the grasshopper optimization algorithm (GOA) and Giza pyramid construction (GPC) under the same operating environment. The results revealed that the proposed AVOA achieved superior economic results toward the least net present cost (\$346,614) and energy price (0.0947 \$/kWh). Moreover, over 20 independent runs, the AVOA showed a better performance in terms of convergence and execution time compared to other tools/algorithms. The obtained findings could be a useful benchmark for researchers in the sizing problem of hybrid energy systems.

Keywords Capacity planning · Metaheuristic optimization · African vultures optimization approach · Energy–economic–environmental analysis · Hybrid renewable energy systems

1 Introduction

1.1 Background and context

In 2019, the number of people without access to electricity reached 770 million who mostly live in sub-Saharan Africa,

rural areas, or developing Asia [1]. Despite the global efforts and progress for the energy access policies to achieve development and sustainable electricity for all, it is estimated that about 670 million people will still lack access to electricity by reaching 2030 [2, 3]. These developments were based only on fossil energy which causes a global fossil energy crisis and environmental problems [4, 5]. Consequently, much focus has been given renewable energy sources (RESs) such as wind, solar, wave, and hydroelectric due to their various advantages such as low running cost, clean, and rich characteristics [6, 7]. The huge development of RESs can be realized in Fig. 1a and b which describes the most recent indicators for both country and technology, respectively [8]. From Fig. 1a, energy generation from PV and wind technologies combined offer about 68% of the RESs. As China stays at the top of the PV market in the world, a significant reduction in new PV facility embellishments occurred

✉ Kotb M. Kotb
kotb.mohamed@f-eng.tanta.edu.eg

¹ Electrical Engineering Department, Faculty of Engineering, Aswan University, Aswan 81542, Egypt

² Electrical Power and Machines Engineering Department, Faculty of Engineering, Tanta University, Tanta 31521, Egypt

³ Renewable Energy Lab, College of Engineering, Prince Sultan University, Riyadh, Saudi Arabia

⁴ Interdisciplinary Research Center for Renewable Energy and Power Systems, King Fahd University of Petroleum and Minerals, Dhahran, Saudi Arabia

in 2020 due to COVID-associated interruptions. RESs are expected to cover 99% of global demand growth by 2025 as shown in the last statistics offered by the IEA in Fig. 2 [7].

Although the wind and solar energies have fast growth, the randomness and intermittence make the system an excessive size when only one energy source is used [9]. Also, this randomness reduces the reliability of the standalone system since the generated energy is influenced by both solar irradiance and wind speed variabilities [10]. Moreover, RESs require a high cost of investment besides the large land area for construction. To overcome the problem of weather variability, energy storage systems (ESSs) are integrated with these sources to form hybrid renewable energy systems (HRESs). Although the use of ESS ensures a steady power supply for load leveling, they increase the total system cost and reduce the energy conversion efficiency [11, 12]. Also, to overcome the cost issue, optimal planning and capacities of systems' components should be accomplished. Recently, HRESs are developed as a green and cost-effective solution for reliability, cost, land area issues, and techno-environmental challenges of conventional sources. The use of the HRESs in standalone or grid-connected applications has been addressed in many studies [15–18]. The optimal capacity planning problem of HRES can be solved using different metaheuristic algorithms (MA) as reviewed in [19, 20], and [21] or via various commercial software tools such as Hybrid Optimization Model for Electric Renewables (HOMER) [22], Hybrid Optimization by Genetic Algorithms (iHOGA) [23], REopt [24], System Advisor Model (SAM) [25], PVWatts [26], and RETScreen [27].

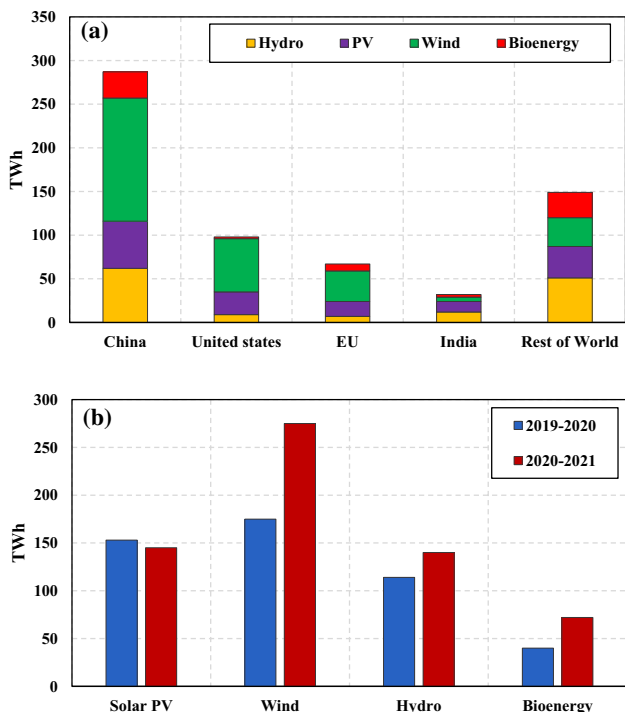


Fig. 1 RESs growth by a country and b technology [8]

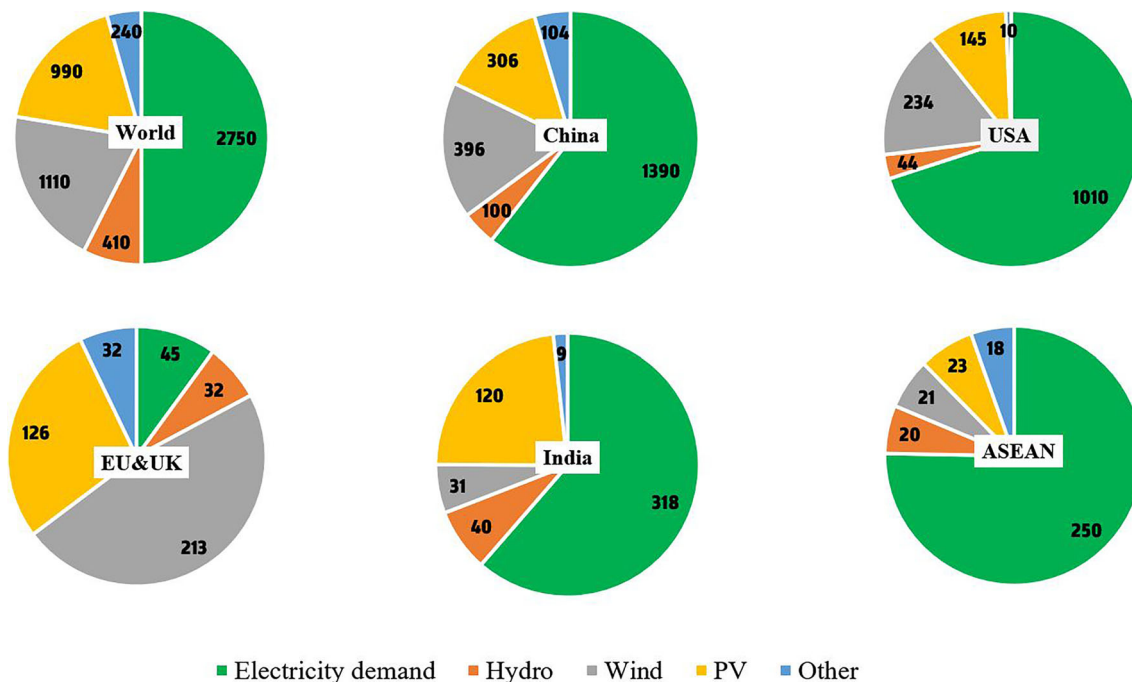


Fig. 2 Growth of electricity demand and RES in TWh between 2019 and 2025 [7]

1.2 Literature survey

Considering the scope of this paper, this survey focuses on studies that employed metaheuristic algorithms, commercial software, or both. Table 1 summarizes the different up-to-date studies that addressed the problem of HRES optimal planning. HOMER software has been widely used in countless research works employing different types of energy solutions for distinct kinds of load demand. For example, the floating PV units were utilized to feed a small electrical system in Bangladesh where the techno-enviro-economic investigations were discussed to present the mini-system profits [28]. In [29], the authors developed a systematic techno-enviro-economic design optimization for a PV, wind, diesel, and batteries energy production system using HOMER. The results revealed that the optimal solution has a TNPC of 351,223 \$ and COE of 0.2262 \$/kWh. In [30], HOMER was used to optimize the cost of 13 scenarios that consist of a hydrogen system, PV, wind, and grid. The authors in [31] used HOMER to investigate optimal solutions regarding the energy, economic, and environmental of an HRES connected with a desalination plant in the new capital airport in Egypt. In another study, the authors in [32] reported using the HOMER software to investigate the techno-economic sustainability of the HRESs using different elements such as PV, wind, pumped hydro storage, diesel, and batteries.

The MA have been broadly used in a wide range of applications in the electric power system; this is due to their various applicability merits [33, 34]. Nevertheless, the applications of the MA are not limited to the field of power systems. In [35], the cyclical parthenogenesis algorithm was employed for layout optimization of truss structures with frequency constraints. Also, the authors in [36] introduced plasma generation optimization as a new physically based metaheuristic algorithm for solving constrained optimization problems. In [37], the dolphin echolocation optimization algorithm was introduced to reduce the computational efforts and time which remain the main challenges that face the MA users. Another efficient metaheuristic optimization algorithm, namely colliding bodies optimization (CBO), was introduced in [38]. The presented algorithm developed straightforward formulation to discover minimum or maximum of functions and does not rely on any interior parameter. Besides, an enhanced version of the CBO algorithm was addressed in [39] for design problems with discrete and continuous variables as well as to escape from local optima dilemma. Likewise, another physically inspired non-gradient algorithm, namely water evaporation optimization (WEO), was developed for solution of global optimization problems to impersonator the evaporation of a small quantity of water particles on the solid exterior [40].

The HOMER and the MA were implemented in different articles to compare and assess their performances. In [41], the

GWO was applied to achieve the optimal techno-economic PV/wind/battery system sizes for Ras Shaitan in Egypt. The obtained results achieved by GWO are compared with those of PSO, WHO, and GA. The study focused only on meeting the load requirements and minimizing the COE. In [42], fuzzy logic controller is used in the GSA to determine the effect of the batteries and diesel systems in the HRESs. In another relevant study [43], the economic and environmental aspects were compromised for hybrid PV/wind energy and batteries using the diesel generator as a spare source. The proposed method is achieved using GA and PSO, and the results are compared with HOMER. The optimal COE and CO₂, which GA and PSO accomplish, have the lowest values compared with that obtained using HOMER software. In [44], the authors proposed a method to optimize the PV, wind, and battery hybrid systems for a specific region in Manipur using a backtrack search algorithm. The obtained results are compared with HOMER by considering the number of wind turbines, PV units, batteries, cost, fluctuation rate, and LPSP. Meanwhile, the authors in [45] used demand–supply management with PSO to design the optimal off-grid system with PV, diesel generator, and battery to energize residential buildings. The results were compared with HOMER considering the economic, technical analyses, and sensitivity evaluation in terms of TNPC, COE, RF, and CO₂.

Recently, AVOA has been proposed and used to achieve different objectives such as tuning the gains, optimal reconfiguration, and optimal sizing [46–48]. In [46], the AVOA is just proposed instead of the PSO to tune the gains of the proportional-integral (PI) controllers for extracting the maximum power from the PV and wind systems. Meanwhile, in [47], the AVOA is adopted in the PV system to overcome the partial shade condition (PSC) where this phenomenon has a negative effect on the PV array which increases the power loss, causes hot spots, and reduces the generated power. Further, in [48], the AVOA is presented to obtain the optimum configuration for a HRESs. The HRESs in this study consist of FC/wind/PV where the grid is the main factor in this investigation. The purpose of this study was to determine the optimal number of HRES components to achieve the lowest TNPC and LOPSP. Although the obtained results have been compared with other MAs, they have not been compared with any commercial software such as HOMER. In addition, the results are used for supplying a building in Ahvaz, Iran, although the main factor was the grid. In [49], an evaluation of PV/WT hybrid renewable energy system forecasting and sizing techniques has been presented.

1.3 Research gaps and contributions

To the best author's knowledge, the proposed AVOA has not been employed before in the optimal sizing of the ISOLATED SYSTEM, which is based on a

Table 1 Recent literature survey on capacity planning of HRESs

References	Year	Location	Structure	Evaluation Metrics				Methodologies		
				E	V	T	R	HOMER	MA	HOMER vs. MA
[28]	2022	Bangladesh	PV/grid	✓	✓	✓	-	✓	-	-
[29]	2020	Egypt	PV/WT/DsG/BESS	✓	✓	✓	-	✓	-	-
[30]	2022	Greece	PV/WT/grid	✓	✓	✓	-	✓	-	-
[31]	2021	Egypt	PV/WT/DsG/BESS/FC	✓	✓	✓	-	✓	-	-
[32]	2021	Canada	PV/WT/DsG/BESS/TPH	✓	✓	✓	-	✓	-	-
[41]	2021	Egypt	PV/WT/BESS	✓	-	✓	-	✓	GWO, PSO, WHO, GA	✓
[50]	2021	Mexico	PV/DsG/BESS	✓	✓	✓	-	✓	NSGA-II	✓
[51]	2022	China	PV/WT/FC	✓	✓	✓	✓	✓	VIKOR	✓
[43]	2021	Egypt	PV/WT/DsG/BESS	✓	✓	-	✓	✓	PSO, GA	✓
[44]	2021	India	PV/WT/BESS	✓	-	✓	-	✓	BSA	✓
[45]	2020	Algeria	PV/WT/DsG/BESS	✓	✓	✓	✓	✓	PSO	✓
[52]	2021	France	PV/WT/BESS	✓	-	-	✓	✓	PSO, GA	✓
[53]	2020	Ecuador	PV/DsG/BESS	✓	-	✓	✓	-	PSO-BPSO	-
[54]	2021	Iran	PV/WT/BESS	✓	-	-	-	-	TS & HS	-
[55]	2018	KSA	PV/WT/DsG/BESS	✓	✓	✓	-	-	MOSaDE	-
[56]	2022	-	PV/WT/BESS	✓	✓	✓	-	-	NSGA-II	-
[57]	2022	India	PV/WT/DsG/BESS	✓	✓	✓	-	✓	PSO, SSA	✓
[58]	2022	-	PV/WT/DsG/BESS	✓	✓	✓	-	✓	HPSODE-FSM	✓
Current	2022	Egypt	PV/WT/DsG/BESS	✓	✓	✓	✓	✓	AVOA, GOA, GPC	✓

PV photovoltaic, WT wind turbine, BESS battery energy storage system, DsG diesel generator, FC fuel cell, TPH turbine-pumped hydro, GA genetic algorithm, PSO particle swarm optimization, BPSO binary particle swarm optimization, TS tabu search, MOSaDE multi-objective optimization using self-adaptive differential evolution, GWO gray wolf optimization, WHO wild horse optimizer, NSGA-II non-dominated sorting genetic algorithm II, SSA salp swarm algorithm, HPSODE-FSM hybrid two-stage PSO-DE optimization-fuzzy satisfaction module, VIKOR Vlekkriterijumsko KOmpromisno Rangiranje, in Serbian, BSA backtracking search algorithm E economic, V environmental, T technical, R reliability

PV/wind/battery/diesel energy system; different attempts have already been accomplished using distinct MA or commercial software (see Table 1). Besides, most existing studies focus only on economic, technical, or environmental objectives or a combination of them, ignoring reliability and emission penalty constraints, except [51]. In addition, there is a lack of depth analysis for both MA and commercial software in depth. Driven from the research gaps, the key contributions of the study can be summarized as follows:

- Developing a robust mathematical model for an autonomous solar/wind/diesel/battery/converter HRES to power the 24-h load demand of a remote urban community in Marsa Matruh city, Egypt, considering actual load and renewable resources data. Meanwhile, presenting an adequate energy management strategy is suggested to coordinate the power flow between various energy sources in RESs which are fully exploited.
- Proposing a new application of the AVOA optimization algorithm to determine the optimal configuration and components' capacities of the HRES under study. The objective function is formulated as multiple objectives to minimize the total net present cost and CO₂ emissions while maintaining the system's loss of power supply reliability at the lowest level.
- Validating and comparing the performance of the AVOA with HOMER, the trusted global standard software in hybrid power system modeling, and up-to-date metaheuristic methods of the grasshopper optimization algorithm (GOA) and the Giza pyramid construction (GPC).
- Providing a systemic and comprehensive energy–economic–environmental analysis of the winning HRES design to understand better the system behavior with the proposed solution based on AVOA.

1.4 Paper organization

Besides the introduction described in Sect. 1, the mathematical models of the proposed HRES components are presented in Sect. 2. The problem formulation and the employed AVOA-based metaheuristic optimization are discussed in Sects. 3 and 4. The obtained simulation and optimization results considering the adopted case study data used are discussed and analyzed in Sects. 5 and 6. Finally, the most important conclusions are summarized in Sect. 7.

2 System description and mathematical modeling

Before the optimization procedure, employing the appropriate mathematical modeling of the PV/WT/DsIG/BESS

hybrid systems illustrated in Fig. 3 is a prerequisite. A description of the technical and economic specifications of the HRES is given in Appendix. Also, the detailed mathematical modeling of each component in the system is offered in Supplementary.

3 Formulation of the design optimization problem

In this section, the design criteria and constraints, as well as the objective function of the optimization problem, are formulated and discussed.

3.1 Design criteria

3.1.1 Total net present cost

Different criteria are used to examine the feasibility and performance of HRES. However, the total net present cost (TNPC) (also called total life cycle cost) approach is yet used as a benchmark criterion for the economic analysis of HRES [50]. This is because TNPC represents all outlay and income costs over the project lifetime by summing the capital cost (CapC), the operating and maintenance cost (O&MC), the replacement cost (RepC), the fuel cost (FuC), and the salvage cost (SavC) as in Eq. (1).

$$\text{TNPC} = \text{CapC} + \text{O\&MC} + \text{RepC} + \text{FuC} - \text{SavC} \quad (1)$$

The entire CapC of the HRES is calculated by Eq. (2) in which $C_{\text{PV_Cap}}$, $C_{\text{WT_Cap}}$, $C_{\text{DsIG_Cap}}$, $C_{\text{BESS_Cap}}$, and $C_{\text{Conv_Cap}}$ are the initial capital costs of the PV, WT, DsIG, BESS, and converter, respectively. Also, N_{PV} , N_{WT} , N_{DsIG} , N_{BESS} , and N_{Conv} are the number of PV modules, WTs, DsIGs, BESS, and converter, respectively.

$$\text{CapC} = (N_{\text{PV}} \times C_{\text{PV_Cap}}) + (N_{\text{WT}} \times C_{\text{WT_Cap}}) + (N_{\text{DsIG}} \times C_{\text{DsIG_Cap}}) + (N_{\text{BESS}} \times C_{\text{BESS_Cap}}) + (N_{\text{Conv}} \times C_{\text{Conv_Cap}}) \quad (2)$$

The FuC of the hybrid system, which is represented in the DsIG, can be calculated by Eq. (3), where FC/yr is the total yearly fuel consumption in liters.

$$\text{FuC} = \text{FC}/\text{yr} \times \sum_{i=1}^N \frac{1}{(1 + D_r)^i} \quad (3)$$

The annual O&MC of the system's components is calculated by Eq. (4) in which $C_{\text{PV_o\&m}}$, $C_{\text{WT_o\&m}}$, $C_{\text{DsIG_o\&m}}$, $C_{\text{BESS_o\&m}}$, and $C_{\text{Conv_o\&m}}$ are the operation and maintenance costs of the PV, WT, DsIG, BESS, and converter, respectively. Also, D_r , N_{oi} , I_r , and N are the discount rate,

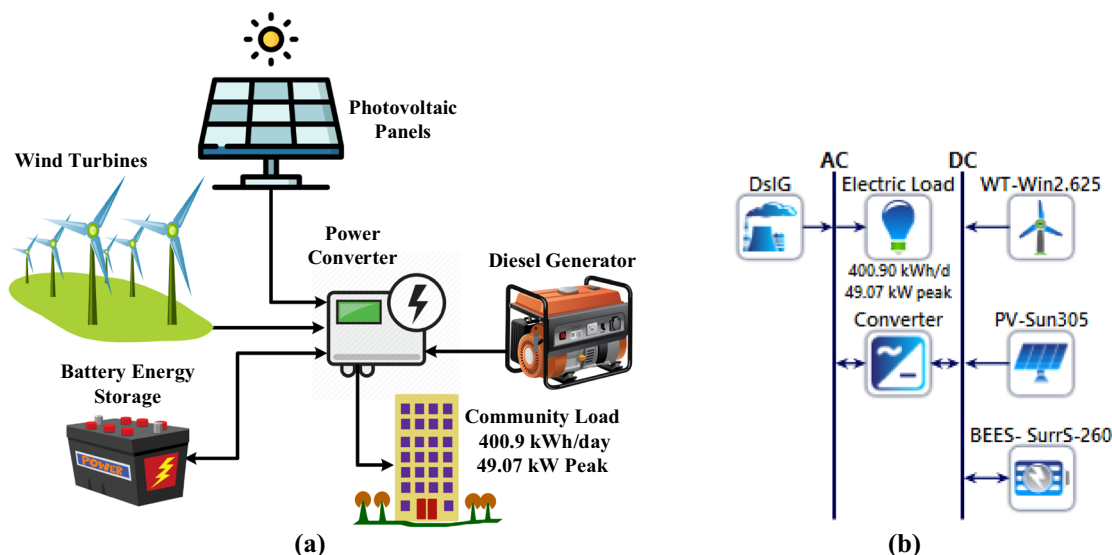


Fig. 3 Representation of the proposed HRES system: **a** schematic diagram and **b** model using HOMER Pro

nominal interest rate, inflation rate, and project lifetime, respectively.

$$\begin{aligned}
 O\&MC = & ((N_{PV} \times C_{PV_o\&m}) + (N_{WT} \times C_{WT_o\&m}) \\
 & + (N_{DsIG} \times (C_{DsIG_o\&m} + FC/yr)) + (N_{BESS} \times C_{BESS_o\&m}) \\
 & + (N_{Conv} \times C_{Conv_o\&m})) \times \sum_{i=1}^N \frac{1}{(1 + D_r)^i} \quad (4)
 \end{aligned}$$

where $D_r = \frac{N_{oi} - I_r}{1 + I_r}$.

Since the lifetime of DsIG, BESS, and the system converter is usually shorter than the project lifetime, they must be substituted at some stage during the project lifetime. Therefore, the RepC of the system’s elements is expressed in Eq. (5) in which C_{DsIG_rep} , C_{BESS_rep} , and C_{Conv_rep} are the replacement costs of the DsIG, BESS, and the converter, respectively. Also, N_c is the lifetime of each component, and N_r is the number of the needed replacement for the system components.

$$\begin{aligned}
 RepC = & \left(N_{DsIG} \times C_{DsIG_rep} \times \sum_{j=1}^{N_r} \frac{1}{(1 + D_r)^{j \times N_c}} \right) \\
 & + \left(N_{BESS} \times C_{BESS_rep} \times \sum_{j=1}^{N_r} \frac{1}{(1 + D_r)^{j \times N_c}} \right) \quad (5) \\
 & + \left(N_{Conv} \times C_{Conv_rep} \times \sum_{j=1}^{N_r} \frac{1}{(1 + D_r)^{j \times N_c}} \right)
 \end{aligned}$$

where $N_r = \lceil \frac{N_c}{N} \rceil - 1$

The salvage cost is the estimated resale value of HRES at the end of its lifetime. It is subtracted from the cost of a fixed asset to determine the amount of the asset cost that

will be depreciated. It can be expressed as given in Eq. (6) where T_{rem} is the remaining time of the component, which is calculated using Eq. (7). The cost data used to calculate the life cycle cost of the HRES are given in Table 10 in Appendix.

$$SavC = \left(\frac{NominalRepC}{(1 + D_r)^N} \right) \left[\frac{T_{rem}}{N_c} \right] \quad (6)$$

$$\begin{aligned}
 T_{rem} = & |N - (\text{last time of replacement} + N_c)| \text{ last time of replacement} \\
 = & N_r * N_c \quad (7)
 \end{aligned}$$

3.1.2 Penalty of emissions

When the diesel generator is running, it produces different harmful gases such as carbon dioxide (CO₂), carbon monoxide (CO), sulfur dioxide (SO₂), and nitrogen oxides. However, carbon dioxide has the dominant quantity, and it harms the surrounding environment. So, the penalty cost of the gas emissions will be applied only to the CO₂ emissions as in Eq. (8) in which PnR (30 \$/ton) is the penalty rate of the environmental policies in the country.

$$PnCE = CO_2 \text{ emissions/yr} \times PnR \quad (8)$$

3.1.3 Cost of energy

The COE is commonly used to calculate the financial viability of HRESs in which the CRF represents the capital recovery factor during the project lifetime, as represented

in Eq. (9) [59].

$$COE = \left(\frac{TNPC + PnCE}{\sum_{t=1}^{8760} E_L(t)} \right) \times CRF \tag{9}$$

where $CRF = \frac{D_r \times (1+D_r)^N}{(1+D_r)^N - 1}$

3.2 Design constraints

3.2.1 Capacity constraints

The capacity constraints of the four components in the system are subjected to the constraints shown in Eq. (10). Besides, $N_{PV,max}$, $N_{WT,max}$, $N_{DslG,max}$, and $N_{BESS,max}$ are the maximum number of PV panels, wind turbines, diesel generators, and batteries, respectively.

$$\begin{cases} 0 \leq N_{PV} \leq N_{PV,max} \\ 0 \leq N_{WT} \leq N_{WT,max} \\ 0 \leq N_{DslG} \leq N_{DslG,max} \\ 0 \leq N_{BESS} \leq N_{BESS,max} \end{cases} \tag{10}$$

3.2.2 Battery lifetime constraints

The energy collected in the BESS is restricted by the state of charge (SOC) limits as represented in Eqs. (11–13) [60], whereas V_{BESS} and C_{BESS} are the BESS’ voltage and rated capacity in Ahr, respectively.

$$E_{BESS,min} \leq E_{BESS}(t) \leq E_{BESS,max} \tag{11}$$

$$E_{BESS,max} = SOC_{BESS,max} \times (N_{BESS} \times V_{BESS} \times C_{BESS}) \tag{12}$$

$$E_{BESS,min} = SOC_{BESS,min} \times (N_{BESS} \times V_{BESS} \times C_{BESS}) \tag{13}$$

3.2.3 Diesel generator operational constraints

Since the performance of the DslG becomes more effective at greater load demand, the minimum necessary load is adjusted at 40% of the DslG nominal power. Consequently, the DslG can work after fulfilling the limitation displayed in Eq. (14) [61] in which η_{Conv} is the converter efficiency.

$$\frac{E_L(t)}{\eta_{Conv}} \geq P_{DslG,rated} \times \Delta t \tag{14}$$

3.2.4 System reliability constraints

Power system reliability is defined as the capability of this system to offer uninterrupted energy for a specific time at particular conditions. The reliability in this study is assessed utilizing the LPSP factor, which is defined by the hourly loss of power supply (HLPS) and hourly energy load demand $E_L(t)$. The HLPS is determined based on the hourly produced energy, load demand, and BESS energy levels. The HLPS and LPSP are calculated using Eqs. (15) and (16), respectively [62]. The objective function is subject to a reliability index of 0% LPSP.

$$HLPS(t) = \frac{E_L(t)}{\eta_{Conv}} - E_G(t) - ((1 - \alpha) \times E_{BESS}(t - 1) - E_{BESS,min}) \times \eta_{rtp} \tag{15}$$

$$LPSP = \frac{\sum_{t=1}^{8760} HLPS(t)}{\sum_{t=1}^{8760} E_L(t)} \tag{16}$$

3.3 Objective function

The objective function for the optimal design of the HRES is formulated to minimize the TNPC in \$ and penalty cost associated with the carbon emission (PnCE) in \$, subject to maintaining various constraints. The summation of the two terms represents the overall cost incurred by the HRES throughout its lifetime period. The objective function for the optimal design of the HRES is formulated to minimize the TNPC and penalty cost associated with the carbon emission subject to various constraints. The objective function (ObjFn) principally hinges on four numeral decision parameters (i.e., number of PV panels (N_{PV}), wind turbines (N_{WT}), diesel generators (N_{DslG}), and batteries (N_{BESS}). The optimization formula is described in Eq. (17).

$$ObjFn = \min LC(N_{PV}, N_{WT}, N_{DslG}, N_{BESS}) = \sum_{e=PV, WT, DslG, BESS, Conv}^{\min} (TNPC + PnCE)_e \tag{17}$$

4 Proposed solution method

4.1 The African vultures optimization algorithm

This approach is one of the metaheuristics that can solve various optimization problems. It has been inspired by the

lifestyle of African vultures [63]. These vultures are considered environmentally beneficial animals that can prevent the carcass from stretching and infecting. Also, they play an important extra-terrestrial role, and their destruction poses several serious risks to human health. They are distributed around the world except in Australia and Antarctica. In recent years, their population has started to decline, and they are more popular in African countries and follow the same lifestyle to find food and sometimes fight each other for food [64]. The African vultures can be split into three categories [65]. The first category includes the vultures, such as the front-footed vulture, which are more likely to be preyed upon than others due to their healthy physical condition. The second category includes vultures that are physically weaker than the first type, such as white-backed African gyphs. The last category includes vultures that are physically weaker than the other two categories, such as the Necrosyrtes monachus hooded vulture. The AVOA follows the behavior of the African vulture during the foraging and navigation behavior to find the optimal solution to a problem. The following subsections will present the steps in the AVOA optimization approach and how AVOA can be used to solve the design challenges of the HRESs in the city of Marsa Matruh.

The complete pseudocode of the AVOA is described in Algorithm 1. It is assumed that N vultures, representing the initial population of a problem, live in a particular environment. Vultures are physically divided into two groups in their natural environment. The first group was designed to compute the fitness function (i.e., objective function) for the entire original population and select the best positions for the first and second vultures. In contrast, the other group forms a population to shift or replace the best two vultures in each presentation. The AVOA optimization algorithm consists of four steps to find the optimal solution to a problem.

4.1.1 Finding the best vulture in any group

The best and second-best vultures are selected after the randomly initial population is evaluated throughout the objective function. At the same time, the other possible solutions move to the first and second groups by using Eq. (18). In addition, a new population is recalculated for each fitness function.

$$R(i) = \begin{cases} \text{BestVulture}_1 & \text{if } p_i = L_1 \\ \text{BestVulture}_2 & \text{if } p_i = L_2 \end{cases} \quad (18)$$

where BestVulture_1 is the best vulture in the first group during the current iteration, BestVulture_2 is the best vulture in the second group during the current iteration, and L_1 and L_2 are the parameters that should be measured before starting the search process and their sum equals one. The probability of

choosing the best solution is determined by selecting each of the best solutions for each group using a roulette wheel, as in Eq. (19), where F is the rate of vultures' starvation.

$$P_i = \frac{F_i}{\sum_{i=1}^n F_i}. \quad (19)$$

Algorithm 1. Pseudocode of AVOA

- 1 **Set** population size (N), the maximum number of
- 2 iterations ($MaxIT$)
- 3 **Initialize** the random population P_i ($i=1,2, \dots, N$)
- 4 **while** (the stopping criteria is not met) **do**
- 5 **Calculate** the fitness function of each Vulture
- 6 **Set** the first best vulture's location $P_{\text{BestVulture}1}$
- 7 **Set** the second-best vulture's location $P_{\text{BestVulture}2}$
- 8 **for** ($i = 1 : N$)
- 9 **Select** $R(i)$ according to Eq. (18)
- 10 **Update** F according to Eq. (21)
- 11 **if** ($|F| \geq 1$) **then**
- 12 **if** ($|P_1| \geq rand_{p1}$) **then**
- 13 **Update** the location of the vulture using Eq. (23)
- 14 **else**
- 15 **Update** the location of the vulture using Eq. (25)
- 16 **if** ($|F| < 1$) **then**
- 17 **if** ($|F| \geq 0.5$) **then**
- 18 **if** ($|P_2| \geq rand_{p2}$) **then**
- 19 **Update** the location of the vulture using Eq. (27)
- 20 **else**
- 21 **Update** the location of the vulture using Eq. (30)
- 22 **else**
- 23 **if** ($|P_3| \geq rand_{p3}$) **then**
- 24 **Update** the location of the vulture using Eq. (33)
- 25 **else**
- 26 **Update** the location of the vulture using Eq. (34)

Return $P_{\text{BestVulture}1}$

4.1.2 Defining the rate of vultures' starvation

A vulture's behavior while searching for prey depends on its energy. When satisfied, vultures can travel long distances in search of prey. However, if they are hungry and unable to find prey due to a lack of flying energy, they will forage

from more closed-up vultures and exhibit aggressive behavior. Satisfaction levels can be modeled using Eqs. (20) and (21).

$$t = h \left(\sin^w \left(\frac{\pi}{2} \frac{i}{\text{MaxIT}} \right) + \cos \left(\frac{\pi}{2} \frac{i}{\text{MaxIT}} \right) - 1 \right) \quad (20)$$

$$F = (2\text{rand}_1 + 1)z \left(1 - \frac{i}{\text{MaxIT}} \right) + t \quad (21)$$

where i is the current iteration number, the MaxIt iteration is the total number of iterations, w is a constant number that should be set before running the AVOA, and both z and h are random numbers. The range of z is $[-1, 1]$, while h is in the range of $[-2, 2]$. When z is greater than zero, the vulture will be satisfied, while the vultures are starved if it is below zero.

4.1.3 Exploration phase

Vultures can travel long distances in search of food for long periods of time. They have high visual abilities and high abilities to detect prey and dry animals. They can explore different random areas using two strategies, where the parameter P_1 can control the selected chosen. Furthermore, P_1 should be randomly selected from the range of $[0, 1]$ before the search operation. In this way, the methodology of these two strategies can be defined by Eqs. (22–25).

$$P(i + 1) = \begin{cases} \text{Eq. (23) if } P_1 \geq \text{rand}_{P_1} \\ \text{Eq. (25) if } P_1 < \text{rand}_{P_1} \end{cases} \quad (22)$$

$$P(i + 1) = R(i) - D(i)F \quad (23)$$

$$D(i) = |XR(i) - P(i)| \quad (24)$$

$$P(i + 1) = R(i) - F + \text{rand}_2((u_b - l_b) \text{rand}_3 + l_b) \quad (25)$$

where $P(i + 1)$ is the position vector of the vulture during the following iteration step, $R(i)$ is one of the best vultures in the current iteration, u_b and l_b are the lower and upper bound of the variables, X is the vultures that move randomly to protect food from other vultures, and rand_3 is a random number to increase the coefficient of random nature while solving the problem.

4.1.4 Exploitation phase

During the exploitation stage, the efficiency of the AVOA can be investigated. Two strategies are available at this stage, depending on the parameters P_2 and P_3 . The parameter P_2 is used for the first phase, while P_2 is employed for the second

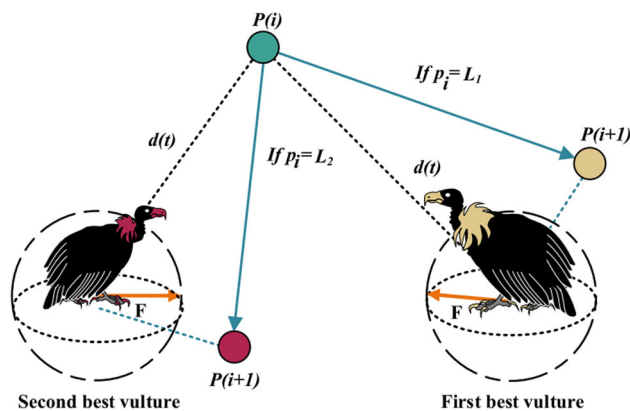


Fig. 4 Food competition for position vectors [63]

phase. These two parameters can have a value between 0 and 1 and must be evaluated before each phase is started.

First phase If the absolute value of F is between 1 and 0.5, then the AVOA enters this first phase. It is controlled by Eq. (26). The powerful vultures do not like to share their prey with other vultures, as shown in Fig. 4. During this time, the weaker vultures will try to feed around the healthy vultures and cause some disturbance, which can be modeled as in Eqs. (27) and (28).

$$P(i + 1) = \begin{cases} \text{Eq. (27) if } P_2 \geq \text{rand}_{P_2} \\ \text{Eq. (30) if } P_2 < \text{rand}_{P_2} \end{cases} \quad (26)$$

$$P(i + 1) = D(i)(F + \text{rand}_4) - d(t) \quad (27)$$

$$d(t) = R(i) - P(i) \quad (28)$$

where $D(i)$ is defined from Eq. (24), $R(i)$ is one of the best vultures of the two groups, $P(i)$ is the current vector position, and rand_4 is a random number between $[0, 1]$ to increase the random coefficient.

Sometimes, during flight, the vultures move in a spiral direction. This spiral model is created between all vultures and the two best vultures, as shown in Fig. 5a, and it can be expressed as in Eqs. (29) and (30).

$$\begin{cases} S_1 = R(i) \left(\frac{\text{rand}_5 P(i)}{2\pi} \right) \cos(P(i)) \\ S_2 = R(i) \left(\frac{\text{rand}_6 P(i)}{2\pi} \right) \sin(P(i)) \end{cases} \quad (29)$$

$$P(i + 1) = R(i) - (S_1 - S_2) \quad (30)$$

where rand_5 and rand_6 are random numbers in the range of $[0, 1]$ to enrich the randomization coefficient.

Second phase In this phase, aggressive food competition is created between the vultures. According to the value of rand_3

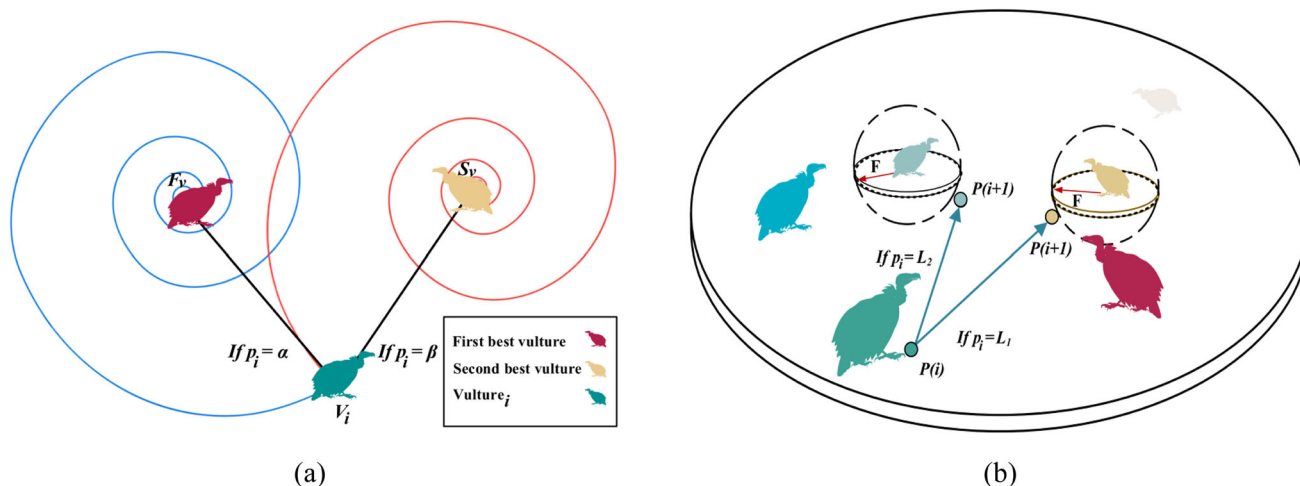


Fig. 5 Position vectors during **a** the rotating flight of vultures and **b** aggressive competition for food [63]

and the parameter P_3 , the next position of a vulture can be defined by Eq. (31).

$$P(i + 1) = \begin{cases} \text{Eq. (33)} & \text{if } P_3 \geq \text{rand}_{P_3} \\ \text{Eq. (34)} & \text{if } P_3 < \text{rand}_{P_3} \end{cases} \quad (31)$$

When vultures are starving and there is huge competition for food, several vulture species can flock to the same food source simultaneously as in Eqs. (32) and (33).

$$\begin{cases} A_1 = \text{BestVulture}_{1(i)} - \frac{\text{BestVulture}_{1(i)} P(i)}{\text{BestVulture}_{1(i)} P(i)^2} F \\ A_2 = \text{BestVulture}_{2(i)} - \frac{\text{BestVulture}_{2(i)} P(i)}{\text{BestVulture}_{2(i)} P(i)^2} F \end{cases} \quad (32)$$

$$P(i + 1) = \frac{A_1 + A_2}{2} \quad (33)$$

The food competition also could be aggressive in this exploitation phase, where the leader vulture becomes starved and weak and loses its energy to fight against other vultures, as shown in Fig. 5b. Then, other vultures start moving toward the leader vulture from different directions as in Eq. (34).

$$P(i + 1) = R(i) - |d(t)| \times F \times \text{levy}(d) \quad (34)$$

where $d(t)$ denotes the distance between the vulture and one of the best vultures in each of the two groups, and levy flight (LF) is used to increase the AVOA’s effectiveness [66] and can be expressed as in Eqs. (35) and (36).

$$\text{LF}(x) = 0.01 \times \frac{u \times \sigma}{|v|^{1/\beta}} \quad (35)$$

$$\sigma = \left(\frac{\Gamma(1 + \beta) \times \sin\left(\frac{\pi\beta}{2}\right)}{\Gamma(1 + \beta^2) \times \beta \times 2\left(\frac{\beta-1}{2}\right)} \right)^{1/\beta} \quad (36)$$

where d denotes the dimensions of the problem, u and v are random numbers between $[0, 1]$, and β is a constant of 1.5.

4.2 Development of AVOA for the optimal HRES design

This part describes integrating the AVOA algorithm to determine the optimal solution to the current optimization problem. The AVOA is a new metaheuristic optimization algorithm motivated by the African vultures’ social behavior, as mentioned earlier. The advantages of AVOA are as follows: easy to implement due to its simple structure, less storage and computational requirements, faster convergence due to continuous reduction of search space; its ability to avoid local minima; and having the ability to find the optimal solutions for problems with nonlinear relationships between its variables, hence better stability, and robustness.

The overall result of this optimization problem is to determine the optimal capacity planning for the city of Marsa Matruh operating in an isolation mode, given the constraints and minimal costs throughout the project lifecycle. An energy management strategy (EMS) is required to coordinate the flow of power between different distributed generations in the system. The proposed EMS is designed according to a cyclic charging strategy as shown in Fig. 6. In this strategy, renewable energy is fully utilized, where it always operates at the maximum power point under current climate conditions. It has a rule-based algorithm in the form of “if” and “then” implementation. Also, the diesel generator has two switched-on or switched-off positions. In this way, when the diesel is running (i.e., switched on), it produces its rated power according to the capacity obtained from the AVOA algorithm. The dummy load is used to absorb the surplus power in the system when charging the BESS to its maximum allowable capacity.

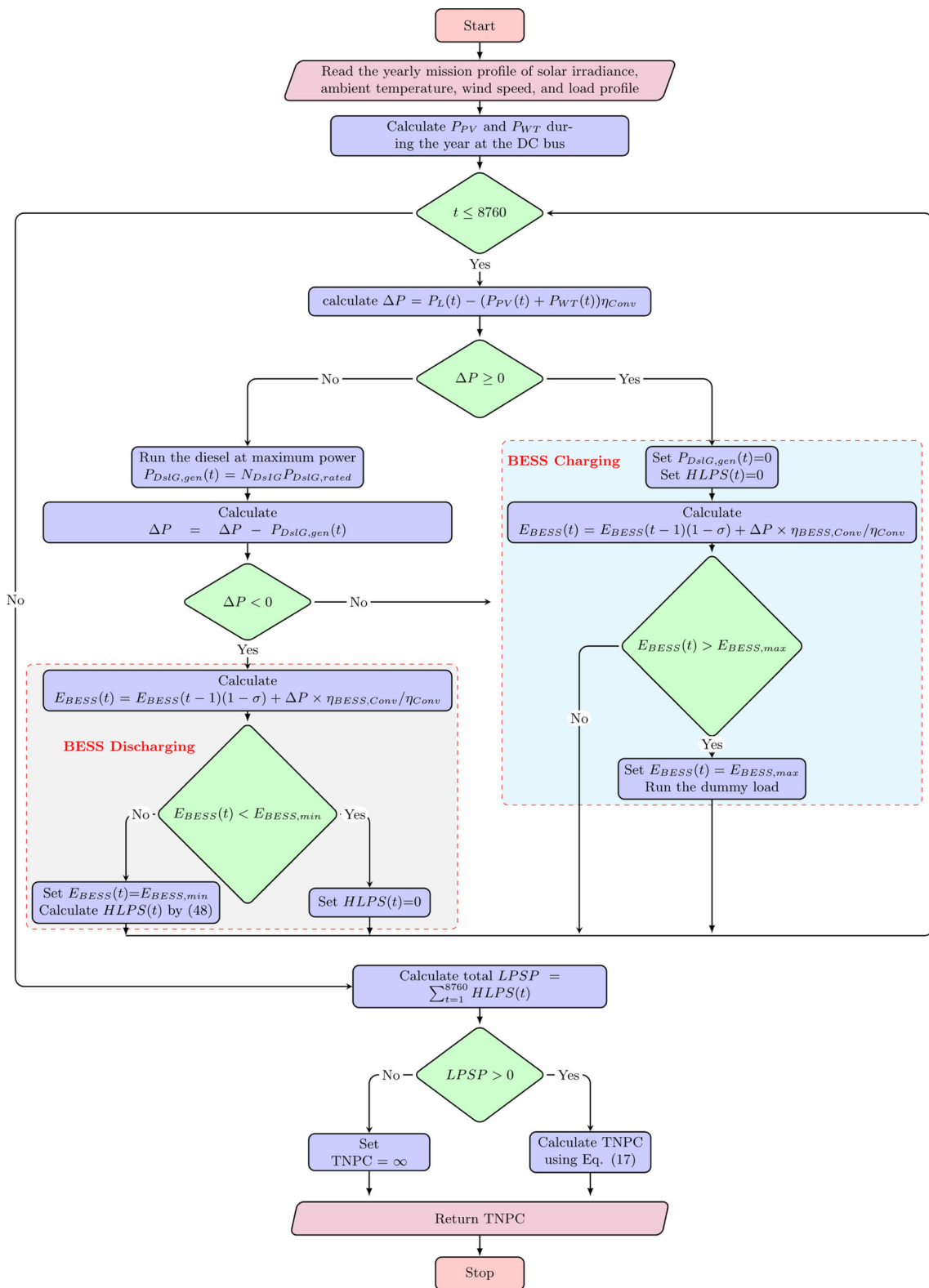


Fig. 6 Overall flowchart of the proposed EMS

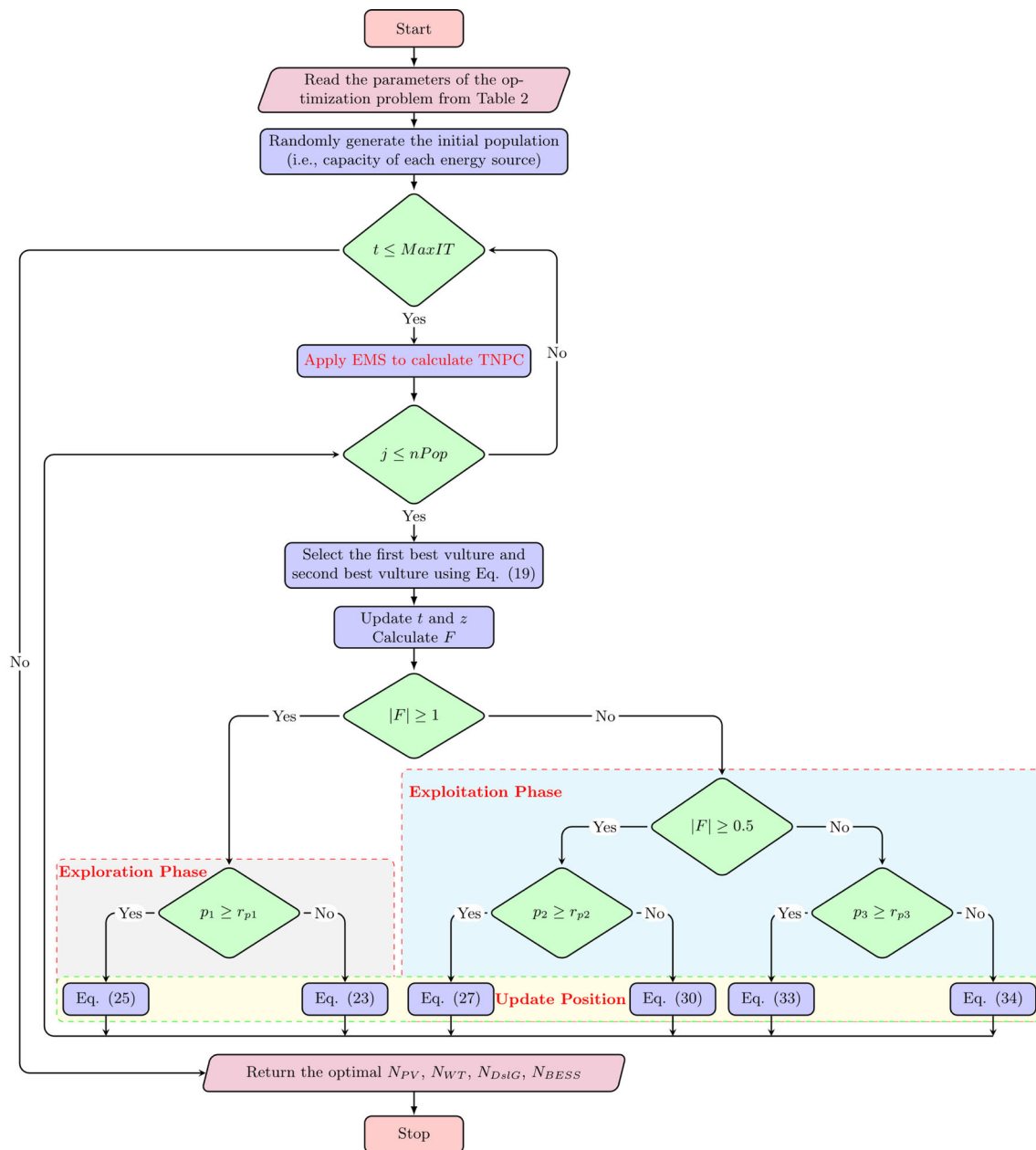


Fig. 7 Complete flowchart of the overall AVOA to solve the current optimization problem

The EMS algorithm starts by calculating the annual available power from the PV and WT based on the given mission profile at the DC bus. Then, the remaining power (ΔP), in the microgrid, can be calculated by subtracting the load, PV, and WT powers at the AC bus to check if the system needs additional power or if there is already surplus power in the system. In the case of $\Delta P > 0$ (that is, extra power is needed), the diesel must operate at its rated capacity to meet the load requirements. At low RESs power and high loading demand, the design maybe not be sufficient to cover all the remaining load demands, which the available power of the BESS should

cover. Furthermore, there could be a load shedding condition, in which the battery cannot deliver at minimum capacity due to lifetime consideration. In such a case, the HLPS should be computed, and it will be greater than zero.

The complete flow diagram clearly illustrating the proposed AVOA for the optimization problem under study is shown in Fig. 7. It starts by loading the input data, such as meteorological data (solar irradiance, ambient temperature, and wind speed) related to the location of the current study. Then, the load demand profile over the year, the technical and economic factors of the HRES components, and the desired

Table 2 Parameters of different optimization approaches in the current study

Item	Value
Number of iterations (MaxIT)	100
Population size ($nPop$)	50
Number of dimensions (dim)	4
Minimum and maximum values (l_b, u_b)	Eq. (37)

limits are also loaded as specified in Sect. 2. The next step is to define the parameters associated with the optimization algorithms, as given in Table 2. The dimension of the current optimization problem consists of four variables: N_{PV} , N_{WT} , N_{DslG} , and N_{BESS} . Finally, the search space of the components' capacity can be listed in Eq. (37).

Fig. 8 Renewable potential in the examined location **a** solar irradiance **b** wind velocity

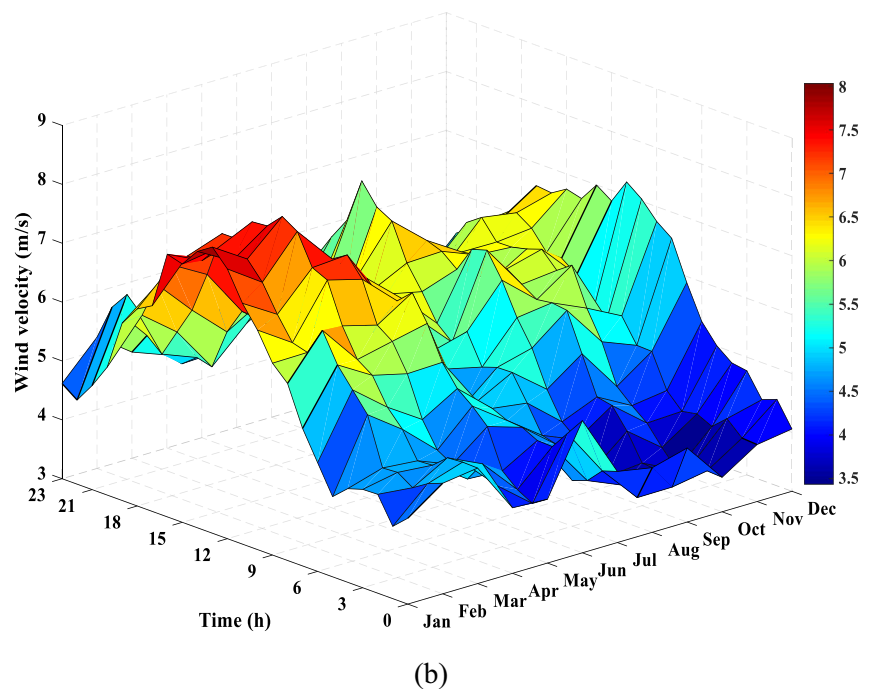
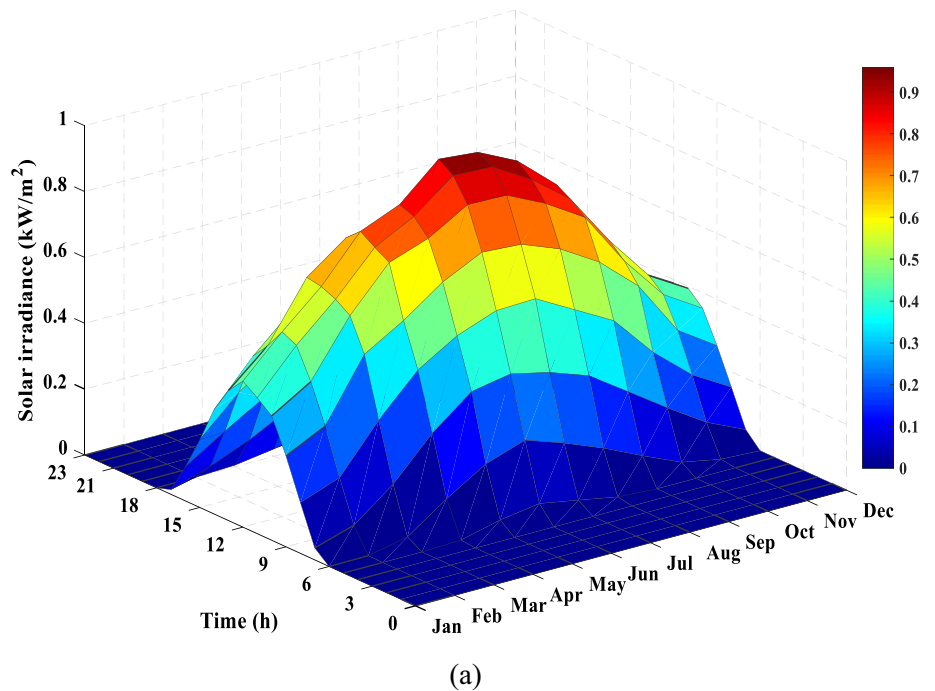
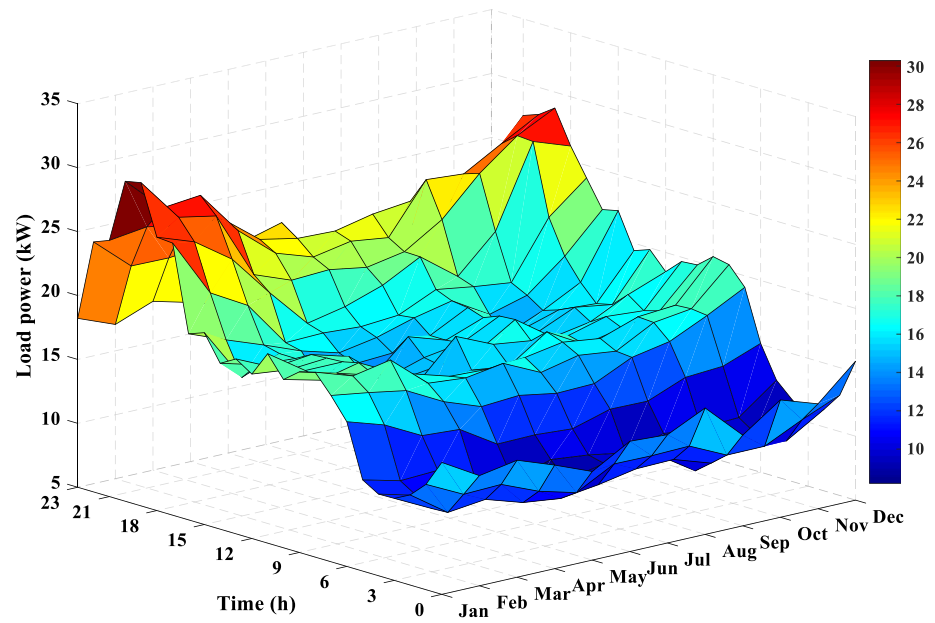


Fig. 9 Hourly, daily, and monthly load power



$$\begin{cases} 0 \leq N_{PV} \leq 200 \\ 0 \leq N_{WT} \leq 200 \\ 0 \leq N_{DslG} \leq 200 \\ 0 \leq N_{BSS} \leq 200 \end{cases} \quad (37)$$

Then, like any metaheuristic approach, a random population set is generated within the search space limit of each dimension. Then, the fitness function is evaluated for each possible candidate in this list to determine the best first and second positions of the vultures. The fitness function will include initial, maintenance, replacement, and salvage costs. Also, to act against climate change, we have included, within the fitness function, the penalty due to carbon emission. To check the feasibility of the proposed optimization method in solving this HRES capacity planning, we have compared it with up-to-date optimization approaches for this type of problem. The comparison algorithms include the GOA [67] and GPC [68]. Their parameters are given in Table 2.

5 Case study

In this study, the proposed AVOA algorithm is tested and validated considering the case study and corresponding input parameters analyzed previously by the authors in [29]. In this previous examination, the design optimization of HRES was performed by HOMER software. This offers the ability to adequately assess and compare the results of the proposed AVOA with the benchmark model of HOMER, in addition to the other applied metaheuristic algorithms of GOA and GPC. The examined locality represents an urban community in Marsa Matruh city (Egypt) at geographical coordinates of

30°54.3'N and 28°23.73'E. The simulated solar irradiance and wind speed profiles of the examined community area, which are collected from the National Aeronautics and Space Administration (NASA) [69], are illustrated in the heat maps given in Fig. 8. Both solar irradiance and wind speed significantly vary each hour, day, and month. From Fig. 8a, the maximum value of the solar irradiance occurs in June with 0.958 kW/m², while the minimum value occurs in December with 0.393-kW/m². Meanwhile, in Fig. 8b, the maximum value of the wind speed occurs in March with 8.03 m/s, while the minimum value occurs in October with 3.43 m/s. The electrical load demand in the examined community represents a group of 60 households, school one school, one healthcare center, two shops, and one community center. The details of the energy consumption of each load are collected from [29].

The hourly, daily, and monthly load demand profile is given in Fig. 9, from which the maximum load demand occurs in January at 30.28 kW while the minimum load demand occurs in September at 8.2 kW. Table 3 summarizes the project's economic input parameters and various adopted technical constraints of the optimization problem. The economic inputs, such as the nominal discount rate and the expected inflation rate, depending on the economic situation of the country where the project is established. They are essentially used to obtain the real discount rate, which converts between the one-time and annualized costs. It is worth mentioning that an emission penalty of 30 \$/ton was assumed in the current study to reflect the environmental policies in the country.

Table 3 Input parameters and constraints of the optimization problem

Input	Value	Constraint	Value (%)
Nominal discount rate	13.25%	Maximum capacity shortage/LPSP	0
Expected inflation rate	4.8%	Minimum renewable fraction	0
Project lifetime	25 years	Operating reserve as % of load	5
System fixed capital cost	0 \$	Operating reserve as % of PV output	5
System fixed O&M cost	0 \$/yr	Operating reserve as % of WT output	5
Capacity shortage penalty	0 \$/kWh	Battery maximum SOC	100
Carbon dioxide penalty	30 \$/ton	Battery minimum SOC	40

6 Results and discussion

In this section, the optimization results of the proposed AVOA are presented and analyzed in detail. For clarifying the efficacy of the presented AVOA, two up-to-date metaheuristic optimization algorithms, the GOA and GPC, and the HOMER optimization software, were also employed to solve the optimization problem, and the results were compared. As mentioned above, the studied HRES was adopted from the investigation accomplished by the authors in [29] using HOMER, but with consideration of emission cost in the objective function.

6.1 Design optimization results

The metaheuristic optimization algorithms are independently executed around 20 times to extract the statistics results, as summarized in Table 4. Therefore, it is obvious that the pro-

Table 4 Statistics of the metaheuristic algorithms for 20 independent runs

Metric	Optimizer		
	AVOA	GOA	GPC
Min	346,614.05	346,685.17	347,222.81
Max	348,073.10	382,924.71	357,824.08
Mean	346,789.82	352,921.34	350,800.81
Median	346,685.17	348,935.70	350,772.36
Std. deviation	319.40	9,995.73	2,484.44
Variance	102,015.78	99,914,630.11	6,172,418.11

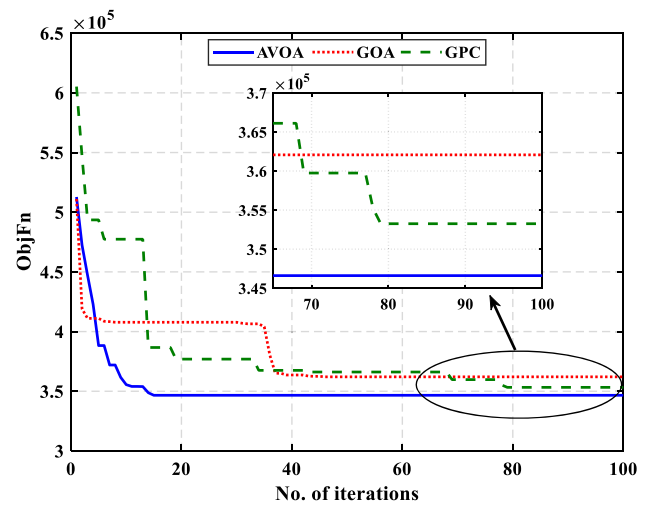


Fig. 10 Convergence of the three adopted metaheuristic algorithms

posed AVOA for optimal HRES design provides the best values compared to GOA and GPC.

The convergence curves of the three adopted algorithms, including the proposed AVOA, GOA, and GPC, are shown in Fig. 10. It can be recognized that the proposed AVOA has a better convergence rate (i.e., the lowest value of the objective function) and statistical measures compared with the GOA and GPC approaches. The algorithms started with initial estimations and remained until the termination condition was fulfilled. Table 5 describes the optimal results of the three metaheuristics optimization algorithms and the HOMER optimizer with their relative ObjFn and execution time. It can be distinguished that the AVOA takes less time than other approaches and attains superior economic results at minimum lifecycle cost (346,614 \$) and energy price (0.0947 \$/kWh). The AVOA reached the optimal solution at the 17th iteration, while the GOA and GPC algorithms found the optimal solution at the 38th and 80th iteration, respectively. The GPC algorithm appears in the second rank, followed by GOA concerning ObjFn, despite taking a longer execution time than the GOA.

Meanwhile, the three optimization algorithms show better financial performance than the HOMER, which gives the highest ObjFn among all methods. For further explanation, Fig. 11 displays the optimal capacities of the different components obtained by the different metaheuristics optimization algorithms and the HOMER software. It can be noticed that the three metaheuristic algorithms did not consider employing WTs in the optimal solution, contrary to the HOMER, which considered 6×2.6 kW WTs. Also, HOMER requires the highest number of batteries (104 units), and thus, the ObjFn resulting from the HOMER will be higher than the other optimization algorithms. Besides, the GOA ranked third due to the high rating required for the PV units (62

Table 5 Comparison of the optimization results of different approaches

	PV kW	WT Qty	DslG kW	BESS Qty	CON kW	ObjFn \$	Execution time Seconds	Rank
AVOA	42	0	27	36	32	346,614	18.66	1
GOA	62	0	22	87	38	362,064	19.51	3
GPC	46	0	31	39	34	353,253	22.76	2
HOMER	43	6	15	104	26.2	370,881	130.6	4

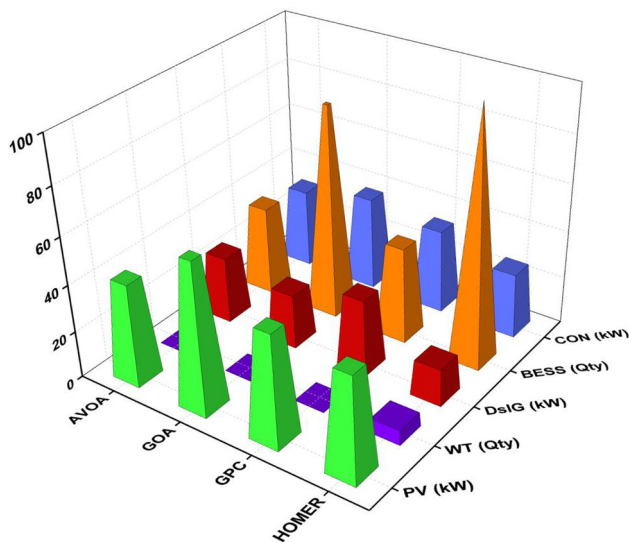


Fig. 11 Optimal capacities of the HRES obtained by the different approaches

kW) and 87 batteries compared to the other metaheuristic algorithms.

6.2 Economic analysis

The detailed economic analysis of the metaheuristic algorithms and HOMER is summarized in Table 6 and portrayed in Fig. 12 for further demonstration. It can be seen that the proposed AVOA has the best optimal cost distribution among all optimizers with the lowest TNPC and LCOE of 346,614 \$ and 0.0947 \$/kWh, respectively. The initial cost of the

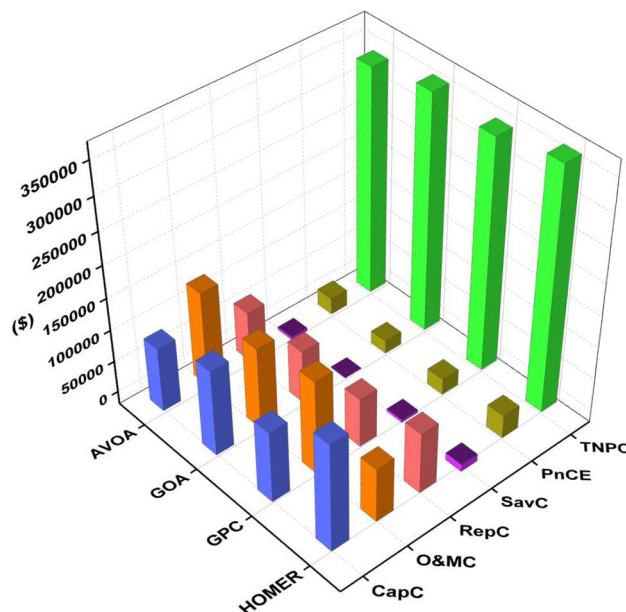


Fig. 12 Illustration of the economic results obtained with AVOA, GOA, GPC, and HOMER

AVOA optimal configuration is fewer than that of HOMER at 40.5%. Besides, the TNPC using the AVOA is reduced by 6.5% compared to HOMER. The optimal configuration suggested by HOMER has an LCOE of 0.239 \$/kWh, while that suggested by the AVOA is 0.0947 \$/kWh, recording a 60.3% reduction. Besides, the suggested LCOE by both the GOA and GPC algorithms is almost the same. It can be distinguished from the obtained results that the AVOA is more efficient than the HOMER and both the GOA and the GPC

Table 6 Detailed economic results of optimized HRES with different approaches

	Cost component (\$)				PnCE (\$)	TNPC (\$)	LCOE (\$/kWh)
	CapC	O&MC	RepC	SavC			
AVOA	99,800	147,681	78,268	4334.1	25,198.4	346,614	0.0947
GOA	134,050	127,159	82,173	1199.6	19,880.9	362,064	0.0990
GPC	110,450	146,133	76,308	4372.9	24,734.6	353,253	0.0966
HOMER	167,859	84,070	94,520	11,402.6	35,833.5	370,881	0.239

Table 7 Cost summary of the optimal system using the different optimizers

Element	Method	CapC	O&MC	RepC	SavC
PV	AVOA	42,000	4460.5	0	0
	GOA	62,000	6584.6	0	0
	GPC	46,000	4885.3	0	0
	HOMER	42,995	4565.1	0	0
WT	AVOA	–	–	–	–
	GOA	–	–	–	–
	GPC	–	–	–	–
	HOMER	60,000	3185.2	11,451.3	5828.1
DslG	AVOA	32,400	136,000	60,991	3719.6
	GOA	26,400	107,299	45,338	469.934
	GPC	37,200	133,495	57,674	3720.1
	HOMER	18,000	83,114	36,839	640.38
BESS	AVOA	12,600	3823.3	13,276	0
	GOA	30,450	9239.7	32,084	0
	GPC	13,650	4141.9	14,382	0
	HOMER	36,400	11,042	42,960	4,432
Conv	AVOA	12,800	3398.5	4001.6	614.42
	GOA	15,200	4035.7	4751.9	729.62
	GPC	13,600	3610.9	4251.7	652.82
	HOMER	10,462	2777.2	3269.5	501.88

algorithms. It is worth mentioning that besides the results convergence of the metaheuristic algorithms with HOMER, the former is further accommodating in control preferences and model advancements. The cost summary of each component in the optimal configuration is also generated from the different optimizers, as summarized in Table 7. It should be noticed that there are no data generated from the metaheuristic algorithms regarding the WT cost since the optimal solution with each algorithm was reached at zero number of WTs. In contrast, the use of HOMER has resulted in six turbines in the optimal solution (see Table 5).

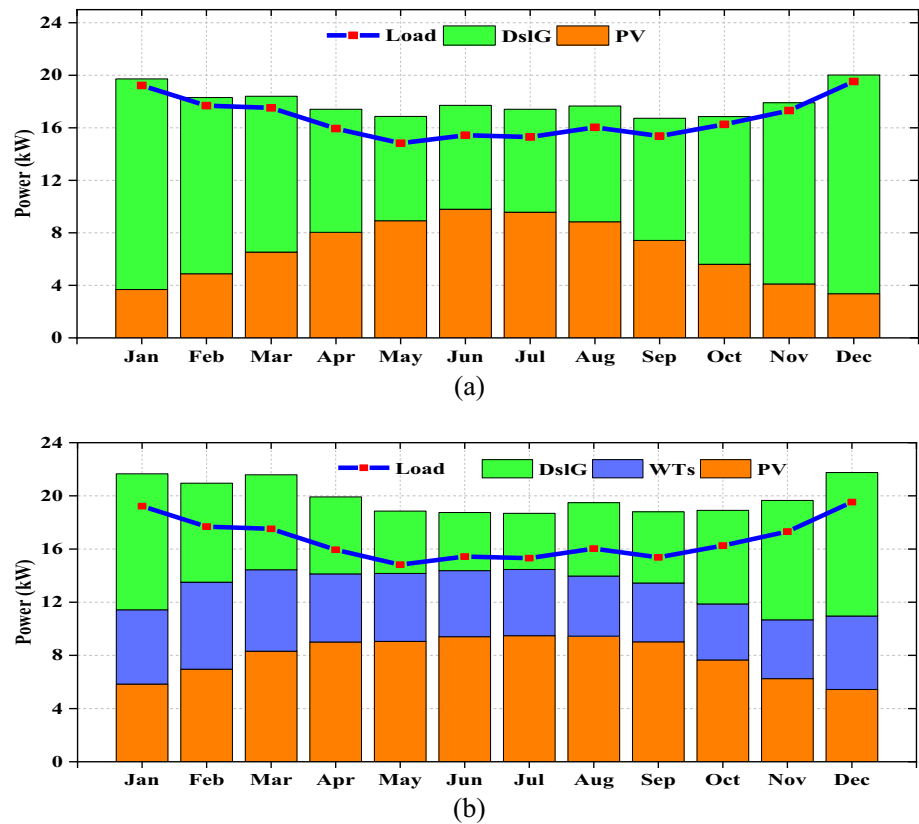
6.3 Energy analysis

The average monthly energy production from the optimized HRES configuration with both the AVOA and HOMER is displayed in Fig. 13. The optimal capacity planning achieved with the AVOA promotes 37.5 and 62.5% energy share from the PV and the DslG, respectively. Meanwhile, the contributions of the PV units, WTs, and DslG in the case of HOMER are 40.1, 25.7, and 34.1% of the total energy produced. As anticipated, it is indicated that the energy production curves for solar and wind generation match the wind speed and solar irradiance profiles in the investigated locality. The figure also reveals that the load demand is efficiently fulfilled using both optimization methods, and the surplus energy is transferred to the batteries.

Moreover, Fig. 14a demonstrates the hourly profile of energy share of the optimal system components and batteries SOC during a year. From Fig. 14a and aided with Fig. 13a, it can be seen that the optimal system candidates by the AVOA share the produced power between the PV system (high share in summertime) and the diesel generator (higher share in wintertime). Besides, samples of two consecutive days during the wintertime and the summertime are indicated in Fig. 14b and c, respectively, from which the energy management and power flow within the optimal system can be verified. Similarly, the hourly profile of energy share using HOMER Pro is indicated in Fig. 15. With a closer view of the yearly profile in Fig. 15a, the SOC of the battery does not have a full charge state which discovers that occasionally the extra power does not transfer to the batteries. The main reason behind this is the kinetic model of batteries utilized by HOMER that relies on the charging/discharging record of the batteries.

Furthermore, the reliability and renewable penetration of the optimal HRES were assessed using three major parameters by the different optimizers: the loss of power supply possibility, the renewable fraction, and the unmet load ratio. Figure 16 shows the results of the different optimizers regarding the discussed parameters. It can be recognized that the three metaheuristic algorithms efficiently served the load demand with zero unmet load ratio, while for HOMER, there is a small portion of the load demand still unserved

Fig. 13 Average monthly contribution of optimal system: **a** AVOA and **b** HOMER



(0.0669%). Because the optimization problem is constrained by a zero-capacity shortage or a zero LPSP, the different optimizers successfully maintained the reliability limits by 0.0067, 0.0002, 0, and 0.0978% for the AVOA, GOA, GPC, and HOMER, respectively. Since the optimal HRES was attained at the highest PV capacity share, the GAO algorithm has the highest renewable fraction ratio (59.6%) among all optimization approaches. A similar value (59.3%) was reached in the case of HOMER owing to the integration of both PV units and WTs in the derived optimal HRES configuration (see Fig. 13). The AVOA and GPC methods have nearly renewable fractions of 40.38 and 44.23%, respectively, due to the conjunction of the PV rating in both methods.

6.4 Emission analysis

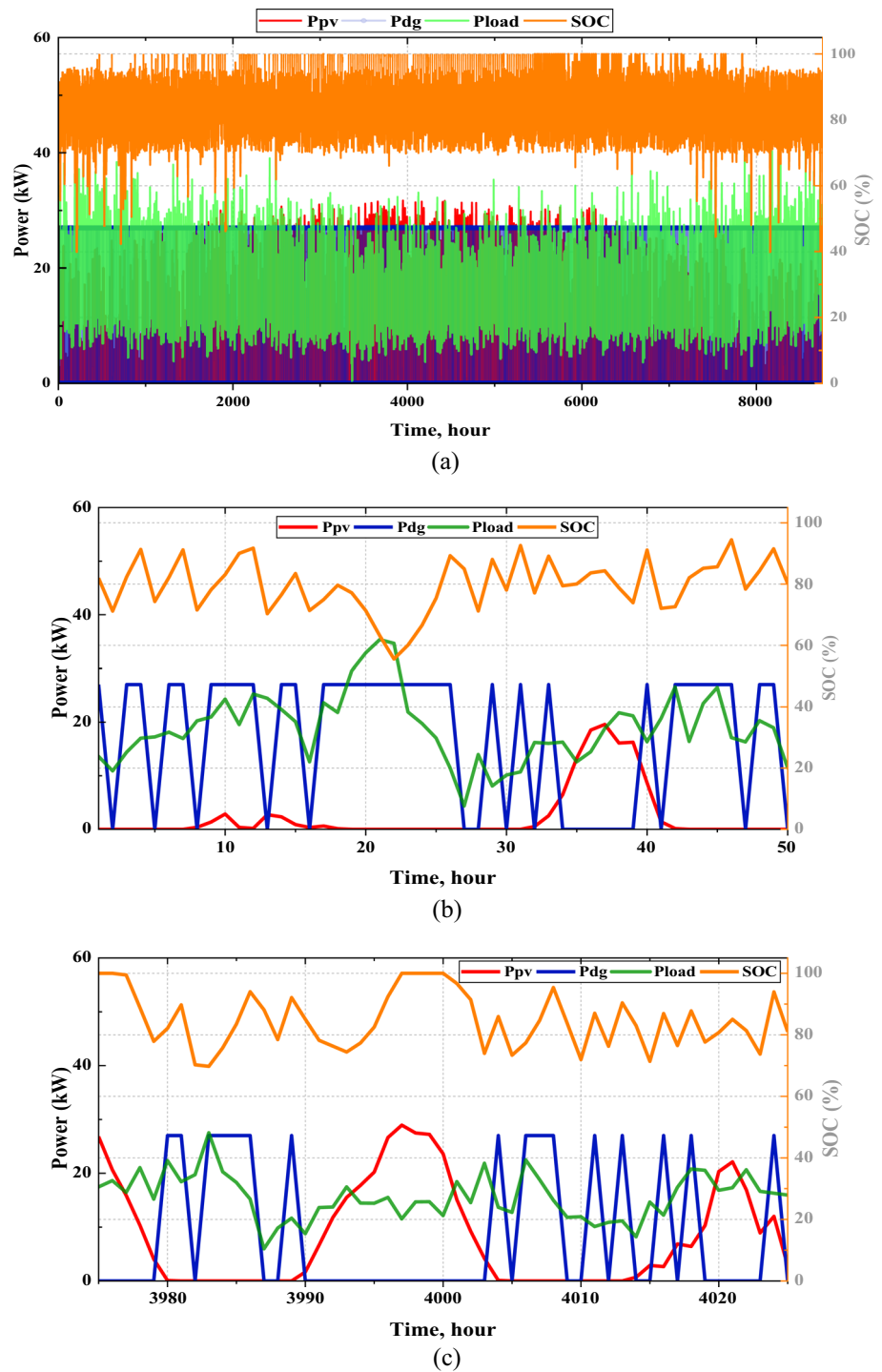
The impact on the environment is also assessed based on the amount of produced CO₂ by the optimal HRES configuration with each solution approach. Table 8 indicates the diesel generator and corresponding CO₂ emission data. The annual amount of CO₂ obtained using the AVOA is estimated at 79,089.1 kg, almost the same resulting from the GPC algorithm. Besides, the amount of CO₂ estimated by HOMER is the lowest at 47,778 kg/year since the projected diesel has the lowest fuel rate consumption with 18,251 L every year.

7 Conclusions and perspectives

This study investigates the feasibility and optimal capacity planning of an autonomous HRESs comprising solar, wind, diesel, and battery sources. The system aims to electrify a remote urban community with 400.09 kWh/day in Marsa Matruh, Egypt. Four optimization approaches include three up-to-date metaheuristic algorithms, AVOA (proposed method), GOA, and GPC, in addition to the HOMER software. The optimization problem is formulated to minimize the TNPC and the emission penalty of HRESs subject to various design and reliability constraints. In addition, the COE, renewable fraction, and unmet load ratio were evaluated and analyzed. The simulation results proved the effectiveness and robustness of the proposed AVOA in applications of hybrid electrical systems under different conditions, as summarized in the following:

- The proposed AVOA algorithm achieved superior results concerning the objective function value compared to other approaches. It achieved a minimum TNPC and PnCE of 346,614\$ and COE (0.0947 \$/kWh), equivalent to 6.5 and 60.4% savings compared to HOMER results, respectively.
- The design based on AVOA efficiently served the load demand with zero LPSP with an acceptable value for a renewable fraction of 40.38%.

Fig. 14 Hourly power sharing of the optimal system using the proposed AVOA: **a** yearly profile, **b** 2 days in winter, and **c** 2 days in summer



- The metaheuristic algorithms showed fast execution time, with AVOA being the first ranked with an average of 18.66 s, followed by GOA (19.51 s) and GPC (7.84 s). In contrast, HOMER has taken significantly longer than the metaheuristic algorithms to find the optimal solution (130 s), which is time-consuming.

Further investigations are recommended for future work, including analyzing new design criteria (e.g., social and technological) in more comprehensive multi-objective optimization. In addition, other active energy management approaches (e.g., demand-side management) could potentially be advantageous in the analyzed research considering the impact of varying the input cost and technical parameters.

Fig. 15 Hourly power sharing of the optimal system using HOMER: **a** yearly profile, **b** 2 days in winter, and **c** 2 days in summer

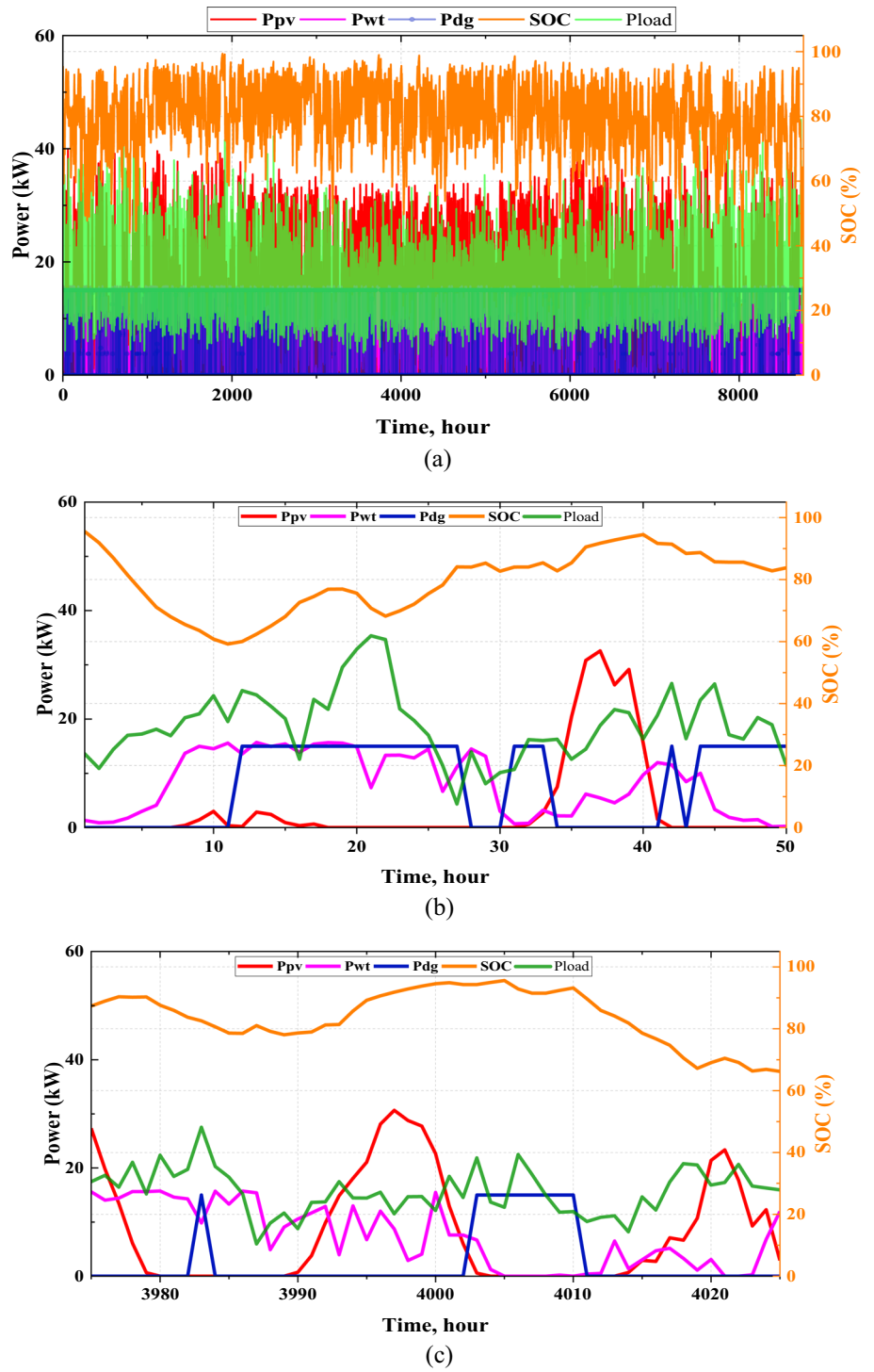


Fig. 16 Reliability and renewable penetration metrics of different optimizers

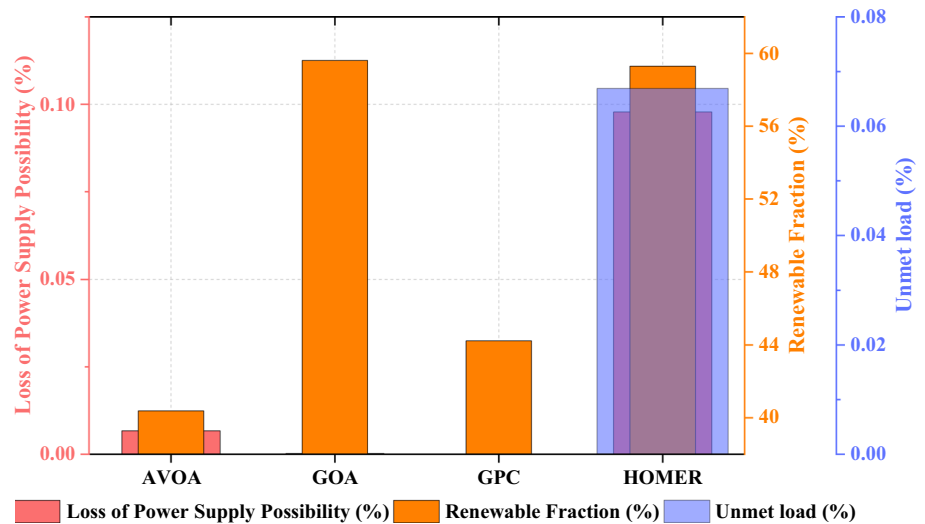


Table 8 DslG and carbon dioxide emission data

	Diesel generator data				CO ₂ emissions (kg/year)
	Capacity (kW)	Hours	Fuel (L/year)	Lifetime (years)	
AVOA	27	3626	29,958	4.13	79,089.1
GOA	22	3511	23,636	4.27	62,399.1
GPC	31	3100	29,406	4.83	77,633.4
HOMER	15	4022	18,251	3.73	47,778

Supplementary Information The online version contains supplementary material available at <https://doi.org/10.1007/s00202-023-01954-9>.

Acknowledgements The authors would like to acknowledge the support of Prince Sultan University during the period of working on the research article.

Author contributions AB was involved in conceptualization, methodology, software, validation, writing—original draft, and writing—review and editing. MFE was involved in resources, investigation, formal analysis, and writing—original draft. HSS was involved in investigation, formal analysis, visualization, writing—original draft, and writing—review and editing. MRE was involved in conceptualization, methodology, validation, and writing—review and editing. DJA was involved in review and editing and supervision. KMK was involved in methodology, software, formal analysis, visualization, writing—original draft, and writing—review and editing.

Funding Open access funding provided by The Science, Technology & Innovation Funding Authority (STDF) in cooperation with The Egyptian Knowledge Bank (EKB).

Declarations

Conflict of interest The authors declare that there is no competing interest. Also, the authors declare that they have no known competing financial interests or personal relationships that could have appeared to influence the work reported in this paper.

Ethical approval Not applicable.

Open Access This article is licensed under a Creative Commons Attribution 4.0 International License, which permits use, sharing, adaptation, distribution and reproduction in any medium or format, as long as you give appropriate credit to the original author(s) and the source, provide a link to the Creative Commons licence, and indicate if changes were made. The images or other third party material in this article are included in the article’s Creative Commons licence, unless indicated otherwise in a credit line to the material. If material is not included in the article’s Creative Commons licence and your intended use is not permitted by statutory regulation or exceeds the permitted use, you will need to obtain permission directly from the copyright holder. To view a copy of this licence, visit <http://creativecommons.org/licenses/by/4.0/>.

Appendix

See Tables 9 and 10.

Table 9 Technical specifications of the studied system

	Item	Value		Item	Value	
PV	Rated capacity/module	305 W	WT	Model type	Tulipo WT	
	Nominal operating temperature	46°C		Rated capacity	2.625 kW	
	Derating factor	85%		Cut-in WS	3 m/s	
	Temperature coefficient	− 0.386%/°C		Cut-out WS	20 m/s	
	Ground reflection	20%		Rated WS	12 m/s	
	Highest system voltage/module	1000 V		Hub height	30 m	
	Open circuit voltage/module	64.2 V		Inertia	7.5 kg m ²	
	Short circuit current/module	5.96 A		Friction coeff	0.06 N m s/rad	
	MPP voltage /module	54.7 V		Lifetime	20 years	
	MPP current/module	5.58 A		Inertia	7.5 kg m ²	
	Working temperature scale	(− 40 to + 85)°C		BESS	Rated voltage	12 V
	Lifetime	25 years			Rated capacity	3.12 kWh
	DslG	Model type		Generic genset	Full capacity	260 Ah
Derating factor		70%	Capacity ratio	0.361		
Heat recovery ratio		0.0%	SOC margins	40–100%		
Fuel curve slope (output)		0.2730 L/hr/kW	DOD	60%		
Intercept coefficient (rated)		0.0330 L/hr/kW	Rate constant	0.379 (1/hr)		
Minimum load ratio		25%	Roundtrip eff	80%		
Carbon monoxide factor		16.34 (g/L)	Max. ch. current	80 A		
Nitrogen oxides factor	15.359 (g/L)	Max. dis. current	80 A			
Converter	Model type	Generic	Lifetime	6 years		
	Efficiency	95%				
	Relative capacity	100%				
	Lifetime	15 years				

Table 10 Cost data of the of the studied system

Component	Capital cost	Replacement cost	O&M cost	Fuel price	Source
PV	1000 \$/kW	1000 \$/kW	10 \$/kW/yr	–	[70]
WT	10,000 \$/unit	9000 \$/turbine	50/unit/yr	–	[71]
DslG	1200 \$/kW	1000 \$/kW	0.039 \$/op.hr/kW	0.3 \$/L	[70–72]
BESS	350 \$/battery	300 \$/battery	10 \$/battery/yr	–	[73]
Converter	400 \$/kW	400 \$/kW	10 \$/kW/yr	–	[74]

References

1. The World Bank: Access to Electricity (% of population) 2022
2. Weinand JM, Scheller F, McKenna R (2020) Reviewing energy system modelling of decentralized energy autonomy. *Energy*. <https://doi.org/10.1016/j.energy.2020.117817>
3. International Energy Agency (2022) Electricity Market Report. Available from: <https://www.iea.org/fuels-and-technologies/electricity>
4. Lian J, Zhang Y, Ma C, Yang Y, Chaima E (2019) A review on recent sizing methodologies of hybrid renewable energy systems. *Energy Convers Manag* 199:112027. <https://doi.org/10.1016/j.enconman.2019.112027>
5. Abdalla AN, Nazir MS, Tao H, Cao S, Ji R, Jiang M et al (2021) Integration of energy storage system and renewable energy sources based on artificial intelligence: an overview. *J Energy Storage*. <https://doi.org/10.1016/j.est.2021.102811>
6. Kotb KM, Elmorshedy MF, Salama HS, Dán A (2022) Enriching the stability of solar/wind DC microgrids using battery and superconducting magnetic energy storage based fuzzy logic control. *J Energy Storage*. <https://doi.org/10.1016/j.est.2021.103751>
7. Renewables 2020 Analysis and forecast to 2025–2020
8. IEA (2021) Global Energy Review 2021, IEA, Paris. <https://www.iea.org/reports/global-energy-review-2021>
9. Prebeg P, Gasparovic G, Krajacic G, Duic N (2016) Long-term energy planning of Croatian power system using multi-objective optimization with focus on renewable energy and integration of electric vehicles. *Appl Energy* 184:1493–1507. <https://doi.org/10.1016/j.apenergy.2016.03.086>
10. Jordehi AR (2018) How to deal with uncertainties in electric power systems? A review. *Renew Sustain Energy Rev* 96:145–155. <https://doi.org/10.1016/J.RSER.2018.07.056>
11. Arani AK, Gharehpetian GB, Abedi M (2019) Review on energy storage systems control methods in microgrids. *Int J Electr Power Energy Syst* 107:745–757. <https://doi.org/10.1016/J.IJEPES.2018.12.040>
12. Kosai S (2019) Dynamic vulnerability in standalone hybrid renewable energy system. *Energy Convers Manag* 180:258–268. <https://doi.org/10.1016/J.ENCONMAN.2018.10.087>
13. Akikur RK, Saidur R, Ping HW, Ullah KR (2013) Comparative study of stand-alone and hybrid solar energy systems suitable for off-grid rural electrification: a review. *Renew Sustain Energy Rev* 27:738–752. <https://doi.org/10.1016/j.rser.2013.06.043>
14. Izadyar N, Ong HC, Chong WT, Leong KY (2016) Resource assessment of the renewable energy potential for a remote area: a review. *Renew Sustain Energy Rev* 62:908–923. <https://doi.org/10.1016/j.rser.2016.05.005>
15. Akbas B, Kocaman AS, Nock D, Trotter PA (2022) Rural electrification: an overview of optimization methods. *Renew Sustain Energy Rev* 156:111935. <https://doi.org/10.1016/j.rser.2021.111935>
16. Bukar AL, Tan CW (2019) A review on stand-alone photovoltaic-wind energy system with fuel cell: system optimization and energy management strategy. *J Clean Prod* 221:73–88. <https://doi.org/10.1016/j.jclepro.2019.02.228>
17. Kotb KM, Said SM, Dán A, Hartmann B (2019) Stability enhancement of isolated-microgrid applying solar power generation using SMES based FLC. In: 2019 7th International Istanbul smart grids and cities congress and fair (ICSG). IEEE, pp 104–108. <https://doi.org/10.1109/SGCF.2019.8782321>
18. Elmorshedy MF, Elkadeem MR, Kotb KM, Taha IBM, Mazzeo D (2021) Optimal design and energy management of an isolated fully renewable energy system integrating batteries and supercapacitors. *Energy Convers Manag* 245:114584. <https://doi.org/10.1016/j.enconman.2021.114584>
19. Diab AAZ, Sultan HM, Kuznetsov ON (2020) Optimal sizing of hybrid solar/wind/hydroelectric pumped storage energy system in Egypt based on different meta-heuristic techniques. *Environ Sci Pollut Res* 27:32318–32340. <https://doi.org/10.1007/s11356-019-06566-0>
20. Zaki Diab AA, Sultan HM, Mohamed IS, Kuznetsov Oleg N, Do TD (2019) Application of different optimization algorithms for optimal sizing of pv/wind/diesel/battery storage stand-alone hybrid microgrid. *IEEE Access* 7:119223–119245. <https://doi.org/10.1109/ACCESS.2019.2936656>
21. Zaki Diab AA, El-Rifaie AM, Zaky MM, Tolba MA (2022) Optimal sizing of stand-alone microgrids based on recent metaheuristic algorithms. *Mathematics*. <https://doi.org/10.3390/math10010140>
22. <https://www.homerenergy.com/products/pro/index.html> (n.d.)
23. Shezan SA (2021) Feasibility analysis of an islanded hybrid wind-diesel-battery microgrid with voltage and power response for offshore Islands. *J Clean Prod* 288:125568. <https://doi.org/10.1016/j.jclepro.2020.125568>
24. Lagrange A, de Simón-Martín M, González-Martínez A, Bracco S, Rosales-Asensio E (2020) Sustainable microgrids with energy storage as a means to increase power resilience in critical facilities: an application to a hospital. *Int J Electr Power Energy Syst* 119:105865. <https://doi.org/10.1016/j.ijepes.2020.105865>
25. <https://sam.nrel.gov/>
26. <https://pvwatts.nrel.gov/>
27. <https://www.nrcan.gc.ca/maps-tools-and-publications/tools/modelling-tools/retscreen/7465>
28. Uddin MN, Biswas MM, Nuruddin S (2022) Techno-economic impacts of floating PV power generation for remote coastal regions. *Sustain Energy Technol Assess* 51:101930. <https://doi.org/10.1016/J.SETA.2021.101930>
29. Kotb KM, Elkadeem MR, Elmorshedy MF, Dán A (2020) Coordinated power management and optimized techno-enviro-economic design of an autonomous hybrid renewable microgrid: a case study in Egypt. *Energy Convers Manag* 221:113185. <https://doi.org/10.1016/j.enconman.2020.113185>
30. Vichos E, Sifakis N, Tsoutsos T (2022) Challenges of integrating hydrogen energy storage systems into nearly zero-energy ports. *Energy* 241:122878. <https://doi.org/10.1016/J.ENERGY.2021.122878>
31. Elkadeem MR, Kotb KM, Elmaadawy K, Ullah Z, Elmolla E, Liu B et al (2021) Feasibility analysis and optimization of an energy-water-heat nexus supplied by an autonomous hybrid renewable power generation system: an empirical study on airport facilities. *Desalination*. <https://doi.org/10.1016/j.desal.2021.114952>
32. Islam MS, Das BK, Das P, Rahaman MH (2021) Techno-economic optimization of a zero emission energy system for a coastal community in Newfoundland, Canada. *Energy* 220:119709. <https://doi.org/10.1016/j.energy.2020.119709>
33. Chicco G, Mazza A (2020) Metaheuristic optimization of power and energy systems: underlying principles and main issues of the ‘rush to heuristics.’ *Energies* 13:5097. <https://doi.org/10.3390/en13195097>
34. Cikan M, Kekezoglu B (2022) Comparison of metaheuristic optimization techniques including Equilibrium optimizer algorithm in power distribution network reconfiguration. *Alex Eng J* 61:991–1031. <https://doi.org/10.1016/j.aej.2021.06.079>
35. Kaveh A, Zolghadr A (2017) Cyclical parthenogenesis algorithm for layout optimization of truss structures with frequency constraints. *Eng Optim* 49:1317–1334. <https://doi.org/10.1080/0305215X.2016.1245730>
36. Kaveh A, Akbari H, Hosseini SM (2021) Plasma generation optimization: a new physically-based metaheuristic algorithm for solving constrained optimization problems. *Eng Comput* 38:1554–1606. <https://doi.org/10.1108/EC-05-2020-0235>

37. Kaveh A, Farhodi N (2013) A new optimization method: dolphin echolocation. *Adv Eng Softw* 59:53–70. <https://doi.org/10.1016/j.advengsoft.2013.03.004>
38. Kaveh A, Mahdavi VR (2014) Colliding bodies optimization: a novel meta-heuristic method. *Comput Struct* 139:18–27. <https://doi.org/10.1016/j.compstruc.2014.04.005>
39. Kaveh A, Ilchi GM (2014) Enhanced colliding bodies optimization for design problems with continuous and discrete variables. *Adv Eng Softw* 77:66–75. <https://doi.org/10.1016/j.advengsoft.2014.08.003>
40. Kaveh A, Bakhshpoori T (2016) Water Evaporation Optimization: a novel physically inspired optimization algorithm. *Comput Struct* 167:69–85. <https://doi.org/10.1016/j.compstruc.2016.01.008>
41. Emad D, El-Hameed MA, El-Fergany AA (2021) Optimal techno-economic design of hybrid PV/wind system comprising battery energy storage: case study for a remote area. *Energy Convers Manag* 249:114847. <https://doi.org/10.1016/j.enconman.2021.114847>
42. Mahmoudi SM, Maleki A, Rezaei OD (2022) A novel method based on fuzzy logic to evaluate the storage and backup systems in determining the optimal size of a hybrid renewable energy system. *J Energy Storage* 49:104015. <https://doi.org/10.1016/j.est.2022.104015>
43. Elnozahy A, Yousef AM, Ghoneim SSM, Abdelwahab SAM, Mohamed M, Abo-Elyousr FK (2021) Optimal economic and environmental indices for hybrid PV/wind-based battery storage system. *J Electr Eng Technol* 16:2847–2862. <https://doi.org/10.1007/S42835-021-00810-9/FIGURES/13>
44. Meitei IC, Pudur R (2021) Optimization of wind solar and battery hybrid renewable system using backtrack search algorithm. *Indones J Electr Eng Comput Sci* 24:1269–1277. <https://doi.org/10.11591/IJEECS.V24.I3.PP1269-1277>
45. Mokhtara C, Negrou B, Bouferrouk A, Yao Y, Setou N, Ramadan M (2020) Integrated supply-demand energy management for optimal design of off-grid hybrid renewable energy systems for residential electrification in arid climates. *Energy Convers Manag* 221:113192. <https://doi.org/10.1016/j.enconman.2020.113192>
46. Ghazi GA, Hasanien HM, Al-Ammar EA, Turkey RA, Ko W, Park S et al (2022) African vulture optimization algorithm-based PI controllers for performance enhancement of hybrid renewable-energy systems. *Sustainability* 14:8172. <https://doi.org/10.3390/su14138172>
47. Alanazi M, Fathy A, Yousri D, Rezk H (2022) Optimal reconfiguration of shaded PV based system using African vultures optimization approach. *Alex Eng J* 61:12159–12185. <https://doi.org/10.1016/j.aej.2022.06.009>
48. Wang Y, Wang J, Yang L, Ma B, Sun G, Youssefi N (2022) Optimal designing of a hybrid renewable energy system connected to an unreliable grid based on enhanced African vulture optimizer. *ISA Trans*. <https://doi.org/10.1016/j.isatra.2022.01.025>
49. Bansal AK (2022) Sizing and forecasting techniques in photovoltaic-wind based hybrid renewable energy system: a review. *J Clean Prod* 369:133376. <https://doi.org/10.1016/j.jclepro.2022.133376>
50. Tariq R, Cetina-Quiñones AJ, Cardoso-Fernández V, Daniela-Abigail HL, Soberanis MAE, Bassam A et al (2021) Artificial intelligence assisted technoeconomic optimization scenarios of hybrid energy systems for water management of an isolated community. *Sustain Energy Technol Assess* 48:101561. <https://doi.org/10.1016/J.SETA.2021.101561>
51. Li X, Gao J, You S, Zheng Y, Zhang Y, Du Q et al (2022) Optimal design and techno-economic analysis of renewable-based multi-carrier energy systems for industries: a case study of a food factory in China. *Energy* 244:123174. <https://doi.org/10.1016/J.ENERGY.2022.123174>
52. Elaoui H, Obeid H, Le Masson S, Foucault O, Gualous H. A comparative study for optimal sizing of a grid-connected hybrid system using Genetic Algorithm, Particle Swarm Optimization, and HOMER. In: IECON 2021–47th annual conference of the IEEE industrial electronics society. <https://doi.org/10.1109/IECON48115.2021.9589999>
53. Llerena-Pizarro O, Proenza-Perez N, Tuna CE, Silveira JL (2020) A PSO-BPSO technique for hybrid power generation system sizing. *IEEE Lat Am Trans* 18:1362–1370. <https://doi.org/10.1109/TLA.2020.9111671>
54. Zhang W, Maleki A, Birjandi AK, Alhuyi Nazari M, Mohammadi O (2021) Discrete optimization algorithm for optimal design of a solar/wind/battery hybrid energy conversion scheme. *Int J Low Carbon Technol* 16:326–340. <https://doi.org/10.1093/ijlct/ctaa067>
55. Ramli MAM, Bouchekara HREH, Alghamdi AS (2018) Optimal sizing of PV/wind/diesel hybrid microgrid system using multi-objective self-adaptive differential evolution algorithm. *Renew Energy* 121:400–411. <https://doi.org/10.1016/j.renene.2018.01.058>
56. Niveditha N, Rajan Singaravel MM (2022) Optimal sizing of hybrid PV–Wind–Battery storage system for Net Zero Energy Buildings to reduce grid burden. *Appl Energy* 324:119713. <https://doi.org/10.1016/j.apenergy.2022.119713>
57. Kushwaha PK, Bhattacharjee C (2022) Integrated techno-economic-enviro-socio design of the hybrid renewable energy system with suitable dispatch strategy for domestic and telecommunication load across India. *J Energy Storage* 55:105340. <https://doi.org/10.1016/j.est.2022.105340>
58. Singh P, Pandit M, Srivastava L (2022) Techno-socio-economic-environmental estimation of hybrid renewable energy system using two-phase swarm-evolutionary algorithm. *Sustain Energy Technol Assess* 53:102483. <https://doi.org/10.1016/j.seta.2022.102483>
59. Bukar AL (2019) Optimal sizing of an autonomous photovoltaic/wind/battery/diesel generator microgrid using grasshopper optimization algorithm. *Sol Energy* 188:685–696
60. Chauhan A, Saini RP (2016) Discrete harmony search based size optimization of Integrated Renewable Energy System for remote rural areas of Uttarakhand state in India. *Renew Energy* 94:587–604. <https://doi.org/10.1016/j.renene.2016.03.079>
61. Tu T, Rajarathnam GP, Vassallo AM (2019) Optimization of a stand-alone photovoltaic e wind e diesel e battery system with multi-layered demand scheduling. *Renew Energy* 131:333–347. <https://doi.org/10.1016/j.renene.2018.07.029>
62. Maleki A (2018) Design and optimization of autonomous solar-wind-reverse osmosis desalination systems coupling battery and hydrogen energy storage by an improved bee algorithm. *Desalination* 435:221–234. <https://doi.org/10.1016/j.desal.2017.05.034>
63. Abdollahzadeh B, Gharehchopogh FS, Mirjalili S (2021) African vultures optimization algorithm: a new nature-inspired metaheuristic algorithm for global optimization problems. *Comput Ind Eng* 158:107408. <https://doi.org/10.1016/J.CIE.2021.107408>
64. Meteyer CU, Rideout BA, Gilbert M, Shivaprasad HL, Oaks JL (2005) Pathology and proposed pathophysiology of diclofenac poisoning in free-living and experimentally exposed oriental white-backed vultures (GYPS bengalensis). *J Wildl Dis* 41:707–716. <https://doi.org/10.7589/0090-3558-41.4.707>
65. Houston DC (1974) The role of griffon vultures Gyps africanus and Gyps ruppellii as scavengers. *J Zool* 172:35–46. <https://doi.org/10.1111/j.1469-7998.1974.tb04092.x>
66. Yang X-SS, Karamanoglu M (2013) Nature-inspired metaheuristic algorithms, 2nd edn. Luniver Press
67. Bukar AL, Tan CW, Yiew LK, Ayop R, Tan WS (2020) A rule-based energy management scheme for long-term optimal capacity planning of grid-independent microgrid optimized by

- multi-objective grasshopper optimization algorithm. *Energy Convers Manag* 221:113161. <https://doi.org/10.1016/J.ENCONMAN.2020.113161>
68. Kharrich M, Kamel S, Alghamdi AS, Eid A, Mosaad MI, Akherraz M et al (2021) Optimal design of an isolated hybrid microgrid for enhanced deployment of renewable energy sources in Saudi Arabia. *Sustainability* 13:4708. <https://doi.org/10.3390/su13094708>
69. <https://www.nasa.gov/>
70. Mousavi SA, Zarchi RA, Astarai FR, Ghasempour R, Khaninezhad FM (2021) Decision-making between renewable energy configurations and grid extension to simultaneously supply electrical power and fresh water in remote villages for five different climate zones. *J Clean Prod* 279:123617. <https://doi.org/10.1016/j.jclepro.2020.123617>
71. Li J, Liu P, Li Z (2020) Optimal design and techno-economic analysis of a solar-wind-biomass off-grid hybrid power system for remote rural electrification: a case study of west China. *Energy* 208:118387. <https://doi.org/10.1016/j.energy.2020.118387>
72. Egypt Diesel prices. GlobalPetrolPrices. https://www.globalpetrolprices.com/Egypt/diesel_prices/. Accessed Dec 2021
73. Cano A, Arévalo P, Jurado F (2020) Energy analysis and techno-economic assessment of a hybrid PV/HKT/BAT system using biomass gasifier: Cuenca-Ecuador case study. *Energy*. <https://doi.org/10.1016/j.energy.2020.117727>
74. Ali F, Ahmar M, Jiang Y, AlAhmad M (2021) A techno-economic assessment of hybrid energy systems in rural Pakistan. *Energy* 215:119103. <https://doi.org/10.1016/j.energy.2020.119103>

Publisher's Note Springer Nature remains neutral with regard to jurisdictional claims in published maps and institutional affiliations.